UC San Diego

UC San Diego Electronic Theses and Dissertations

Title

Biophysical characterization of p53 regulatory domain and MDM2

Permalink

https://escholarship.org/uc/item/6xd7g1q5

Author

Cheung, Nikki Hoi Ling

Publication Date

2010

Peer reviewed|Thesis/dissertation

eScholarship.org Powered by the California Digital Library
University of California

UNIVERSITY OF CALIFORNIA, SAN DIEGO

Biophysical Characterization of p53 regulatory domain and MDM2

A Thesis submitted in partial satisfaction of the
requirements for the degree Master of Science

in

Chemistry

by

Nikki Hoi Ling Cheung

Committee in charge:

Professor Hector Viadiu, Chair
Professor Susan S. Taylor
Professor Daniel J. Donoghue

2010

Copyright

Nikki Hoi Ling Cheung, 2010

All rights reserved.

The Thesis of Nikki Hoi Ling Cheung is approved and it is acceptable in quality and form for publication on microfilm and electronically:

Chair

University of California, San Diego

2010

TABLE OF CONTENTS

Signature Page……. iii

Table of Contents……. iv

List of Symbols and Abbreviations……..……..…… vi

List of Figures……...……..……... viii

List of Tables……...……...…… x

Acknowledgements……...……...…….. xi

Abstract of the Thesis……. xii

Chapter One……...……...…….. 1

Introduction

What is p53? ……...…...…… 2
The p53 Pathway……...…...…… 3
Structure of p53……...……...…… 4
Efforts towards p53 Structures……...……..…… 6
Objectives of Thesis…… 8
References……...…… 13

Chapter Two……...……..……... 17

Structural Studies and Biophysical Characterization of p53CTD

Introduction……...…… 18
Materials and Methods…… 21
Results……...…… 28
Discussion……. 49
References…… 50

Chapter Three…… 53

Expression and Purification of p53 Variants

Introduction…… 54
Materials and Methods…… 56
Results…… 57
Discussion…… 63
References…… 64

Chapter Four…… 65

Understanding the Oligomerization State of MDM2 by Analytical

Ultracentrifugation and Electron Microscopy

Introduction…… 66
Materials and Methods…… 73
Results…… 76
Discussion…… 83
References…… 84

LIST OF SYMBOLS AND ABBREVIATIONS

Å	Angstrom
ACV	Acetonitrile
Ala	Alanine
ATM	Ataxia telangiectasia mutated kinase
Arg	Arginine
AUC	Analytical Ultracentrifugation
β-ME	Beta mercaptoethanol
bp	Bair pair
CAD	Central Acidic Domain
CBP	CREB Binding Protein
CD	Circular Dichroism
Chk-2	Checkpoint kinase 2
Da	Dalton
DNA-PK	DNA-dependent protein kinase
DND	DNA Binding Domain
DTT	Dithiothreitol
E.coli	Escherichia coli
Gln	Glutamine
Gly	Glycine
IPTG	Isopropyl β-D-1-thiogalactopyranoside
Ile	Isoleucine
kDa	Kilodalton

Leu	Leucine
MBP	Maltose Binding Protein
MDM2	Murine Double Minute 2
mM	millimolar
NaCl	Sodium Chloride
Na_2HPO_4	Sodium Phosphate
NMR	Nuclear Magnetic Resonance
OD	Optical Density
Phe	Phenylalanine
PMSF	Phenylmethanesulfonylfluoride
Pro	Proline
Pu	Purine
r.p.m.	Revolution per minute
SDS-PAGE	Sodium Dodecyl Sulfate Polyacrylamide Gel Electrophoresis
Sw	Sedimentation Coefficient
TAD	Transactivation Domain
TEM	Transmission Electron Microscopy
Tris HCl	Tris Hydrochloride
Try	Tyrosine
Val	Valine

LIST OF FIGURES

Figure 1.1. Domain Organization of Human p53 sequence…… 10
Figure 1.2. A model of the p53 pathway…… 12
Figure 2.1. Domain organization and sequence of p53CTD…… 20
Figure 2.2. SDS-PAGE Analysis of MBP-pp-p53CTD Purification…… 33
Figure 2.3. MonoS Elution Profile of p53CTD……..... 34
Figure 2.4. Gel Filtration Profile of p53CTD using G25……..... 35
Figure 2.5. MALDI-TOF Spectrum of SeMeth p53CTD before crystallization 36
Figure 2.6. MALDI-TOF Spectrum of p53CTD dissolved crystal…… 37
Figure 2.7. p53CTD crystal……..... 38
Figure 2.8. One degree oscillation diffraction pattern of p53CTD crystal collected at SSRL BL7-1…… 38
Figure 2.9. Crystal packing of p53CTD…… 39
Figure 2.10. $|2F_o-F_c|$ electron density map of p53CTD dimer…… 39
Figure 2.11. Dimer of p53CTD observed in the unit cell…… 40
Figure 2.12. Tetramerized state of p53CTD…….. 40
Figure 2.13. Hydrophobic core of p53 tetramerization domain…… 41
Figure 2.14. SDS-PAGE analysis of purification of MBP-pp-p53CTD G360S/G361 mutant…… 42
Figure 2.15. SDS-PAGE analysis of digested MBP-pp-p53CTD mutant..... 43
Figure 2.16. Sedimentation Distribution of p53CTD obtained by SEDFIT program…… 45
Figure 2.17. Sedimentation Distribution of p53CTD and p53CTD complexed with specific 14 b.p. DNA obtained by SEDFIT program..... 46
Figure 2.18. Sedimentation Distribution of p53CTD and p53CTD complexed with non-specific 14 b.p. DNA obtained by SEDFIT program….. 47
Figure 2.19. Sedimentation Distribution of p53CTD and p53CTD complexed with specific 24 b.p. DNA obtained by SEDFIT program…… 48
Figure 3.1. Domain Organization of p53 variants……..... 55
Figure 3.2. SDS-PAGE analysis of 8xHis-tagged full length p53 purification 59

Figure 3.3. Western analysis of 8xHis-tagged full length p53 purification..... 60
Figure 3.4. SDS-PAGE analysis of MBP-pp-p53 94-393 purification..... 61
Figure 3.5. SDS-PAGE analysis of MBP-pp-p53 94-393 Δ28 purification….. 62
Figure 4.1. MDM2 in resting cells…….. 70
Figure 4.2. MDM2 after DNA damage……..…….. 71
Figure 4.3. Domain Orgainzation of Human MDM2…… 72
Figure 4.4. SDS-PAGE analysis of purification of 8xHis-MDM2……..…. 79
Figure 4.5-1. Peptides of MDM2 analyzed by tandem mass spectrometry…..... 80
Figure 4.5-2. Result of electrospray ionization of 8xHis-MDM2 using Tandem Mass Spectrometry (MS/MS)……...……. 80
Figure 4.6. Chromatogram of samples purified from Superose 6 column along with SDS-PAGE analysis……..…….. 81
Figure 4.7. Sedimentation Distribution of 8xHis-MDM2……...……. 82
Figure 4.8. Average of MDM2 particles……...……..……. 82

LIST OF TABLES

Table 1.1. Recent and Highlighted p53 Structures Determination…… 11
Table 2.1. Data Collection Table of p53CTD crystal…….…….. 27
Table 2.2. Summary of DNA sequences using in the study of the interaction of p53CTD with DNA…….……...……...……...…..…… 44
Table 2.3. Summary of Sedimentation Distribution of p53CTD and p53CTD with Specific 14 b.p. DNA……...…… 46
Table 2.4. Summary of Sedimentation Distribution of p53CTD and p53CTD with non-specific 14 b.p. DNA……..…… 47
Table 2.5. Summary of Sedimentation Distribution of p53CTD and p53CTD with specific 24 b.p. DNA …….…… 48

ACKNOWLEDGEMENTS

First and foremost I offer my sincerest gratitude to my supervisor, Dr. Hector Viadiu for his mentorship, support and encouragement throughout my graduate studies. His enthusiasm and passion in science exceptionally inspired and enriched my growth as a student, a researcher, and a scientist. Without his guidance and persistent help, this thesis would not have been possible. My fellow lab members, past and present, have been helpful along the way. I am heartily thankful to my undergraduate supervisor, Dr. Susan Taylor, who provided me an opportunity to pursue my undergraduate research career. I have been amazingly fortunate to have an advisor, Dr. Choel Kim, who introduced me to the field of studying protein structure by X-ray crystallography and taught me biochemical techniques. Without the help of Dr. Abdul Ethayathulla, much of the structural work in this project would not have been possible. His work is greatly appreciated. I would like to thank Dr. Majid Ghassemian for helping with MS/MS data collection. I am also indebted to my special friends Aki Tse and Vivien Wang for being so supportive and tremendously helpful in many areas throughout these years. I gratefully thank two undergraduates, Kate Kim and Tracy Truong, for help in protein expression and continuing research in these areas. I would also like to thank Michelle Chan for help in electron microscopy. In addition, I offer my regards and blessings to all of those who supported me in any respect during the completion of this project. Lastly, I thank my parents and my sister for their love and support across the Pacific.

ABSTRACT OF THE THESIS

Biophysical Characterization of p53 regulatory domain and MDM2

by

Nikki Hoi Ling Cheung

Master of Science in Chemistry

University of California, San Diego, 2010

Professor Hector Viadiu, Chair

p53 tumor suppressor protein plays a central role in responding to DNA damage by activating DNA repair, cell cycle arrest, senescence or apoptosis. In resting cells, MDM2 negatively regulates p53 by both blocking p53-coactivator interactions, as well as promoting p53 ubiquitin-dependent proteasomal degradation. In stressed cells, p53 transcriptional activity is positively regulated by its own C-terminal regulatory domain through non-specific DNA interactions that enhance specific DNA binding through the DNA binding domain. Mutations in p53 DNA binding domain and upregulation of MDM2 are involved in 50% of cancer cases. Understanding p53 and MDM2 at molecular level is crucial to design pharmacological targets to fight cancerous cells. However, structures of full-length of p53 and MDM2 have not yet been determined. The first goal of this

thesis is to understand the DNA binding properties and crystal structure of the two most C-terminal domains of p53 (p53CTD) that include the tetramerization and regulatory domains. Our analytical centrifugation results indicated that p53 CTD binds to specific and non-specific DNA and that it changes from tetrameric state to dimeric state upon DNA binding. Our second goal is to understand the oligomerization state of MDM2 using AUC and transmission electron microscopy. Our results indicated that recombinant full-length MDM2 self-assembles to forms spherical particles of different sizes formed by different oligomerization.

Chapter One

Introduction

Around 50 percent of cancer patients are living with a tumor that contains an inactivating mutation on the human gene p53. The majority of cancers of ovary, esophagus, colorectum, head and neck and pancreas present p53 mutations (Olivier et al., 2002). Moreover, 30% of cancer cells in lung, skin, bladder, stomach, brain and liver also carry mutations in a p53 allele (Olivier et al., 2002). A majority of tumors also present inactivation of other proteins that partially abrogate the p53 pathway (Brown et al., 2009). Since p53 is one of the most frequently mutated genes in human cancer, p53 and its associated proteins are therefore prime targets for developing new cancer drugs. Detailed structural and biophysical studies of the molecular interactions in the p53 signaling pathway are crucial to our ability to intervene pharmacologically in cancer cases.

1.1 What is p53?

p53 is a transcription factor that has a tumor suppressor activity because it acts as a critical mediator in the cell signaling pathway that respond to DNA damage. It is known as the "guardian of the genome" because it prevents cells with damaged DNA from proliferating. When p53 is active, it may inhibit cell division in one of several ways, including activating the caspase apoptotic pathway, activating p21 in cell cycle arrest, or inducing senescence (Oren, 2003, Toledo and Wahl, 2006, Gatz and Wiesmuller, 2006, Vogelstein et al., 2000). Both intrinsic and extrinsic stresses can induce activation of p53 by post-translational modifications such as phosphorylation, acetylation or methylation. Active p53 binds specific DNA binding elements on the promoter of its target

genes to trigger gene activation by recruiting the rest of the transcription machinery.

1.2 The p53 Pathway

At the level of p53 multiple upstream signals from many pathways converge and p53 also down-regulates several pathways. During homeostasis, the N-terminus of MDM2 (Murine Double Minute 2) binds to p53 transactivation domain, promoting the polyubiquitination of p53 C-terminus triggering its degradation by the proteosome. Notably, the level of p53 in cells depends mostly on its degradation rate, rather than the synthesis rate (Vogelstein et al., 2000). In response to DNA damage, p53 transactivation domain (TAD) is phosphorylated by several kinases such as Chk2, DNA PK, or ATM inducing the recruitment of the transcriptional coactivator p300/CBP and other factors of the transcription machinery that activate p53 target genes (Lavin and Gueven, 2006, Itahana et al., 2009). The phosphorylation of p53 TAD prevents p53 binding to MDM2, stabilizing p53 and increasing its cellular levels (Itahana et al., 2007). A recent study using NMR and fluorescence anisotropy confirms that p300/CBP wraps around the p53 tetramer to promote acetylation at multiple lysine residues (residues 370, 372, 373, 381, and 382) in the regulatory domain of p53 (Itahana et al., 2009). Such modifications enhance p53 sequence-specific DNA binding affinity and promote transcription of target genes by recruiting transcription activators (Itahana et al., 2008) (Figure 1b).

1.3 Structure of p53

Human p53 is a polypeptide chain of 393 amino acids, consisting of five major domains: transactivation domain, proline rich region, DNA binding domain, tetramerization domain and regulatory domain. Each domain has distinct features, but all domains are interdependent on each other for a complete function (Figure 1a).

Transactivation Domain

The transactivation domain (TAD, residues 1-65) is located at the N-terminus of p53. This domain is rich in glutamic acid and aspartic acid residues (Viadiu, 2008). p53 TAD domain can facilitate transcription activity and regulate p53 function by interacting with transcription coactivators such as p300/CBP and p21 (Joerger and Fersht, 2008, Stavridi, 2005). It is also involved in negative regulation of p53 by interacting with the ubiquitin E3 ligase protein MDM2. In this region, the binding sites for p300 and MDM2 overlap (Stavridi et al., 2005). In steady state, MDM2 binds to the TAD and maintains p53 at basal levels by promoting ubiquitin-dependent proteasomal degradation. Upon DNA damage, p53 TAD is phosphorylated by protein kinases decreasing the affinity of the p53/MDM2 interaction. This leads to an increased level of p53 that facilitates p300/CBP recruitment to increase transcriptional activity (Joerger et al., 2008).

DNA Binding Domain

After the TAD domain gets phosphorylated, p53 binds to its specific promoter sequence via the DNA binding domain (DBD, residues 93-292) (Jeffrey et al., 1995). p53 DBD binds to a 20 bp consensus DNA sequence consisting of four Pu-Pu-Pu-C-A/T repeats (Bargonetti et al., 1991). Previous studies have shown that mutations in DBD have drastic negative effects on p53 transcriptional activity (Stavridi, 2005, Viadiu, 2008). The majority of these mutations are missense mutations and can be divided into two classes. Class I mutants are frequently found in residues that involve direct DNA contacts, such as Arg248 and Arg273. Class II mutants are frequently found in residues which regulate the stability of the DBD, such as Arg175, Arg249, and Arg282 (Stavridi et al., 2005).

Tetramerization Domain

The tetramerization domain (TD, residues 324-361) resides near the C-terminus, which holds four p53 monomers together through hydrophobic interactions between side chains of Ile332, Phe338 and Phe341. It is interesting to note that tetramerization is not required for p53 DNA binding *in vitro*. However, DBD alone has approximately five-fold less the DNA binding affinity compared to the intact tetrameric p53 (Jeffrey et al., 1995, Pavletich et al., 1993). Each tetramerization domain consists of a β strand (residue 326 to 333) and an α helix (residue 335 to 354), which form two sides of a V-shaped structure, connected by a Gly334 hinge (Jeffrey et al., 1995).

Regulatory Domain

The p53 regulatory domain consists of the last 30 amino acids and is located at the extreme C-terminus. This region is rich in lysines and arginines (Viadiu, 2008). Previous studies have shown that this domain is subject to multiple post-translational modifications such as ubiquitination, methylation and acetylation, which are important for p53 down-regulation (Xu, 2003, Appella and Anderson, 2000, Brooks and Gu, 2003, Stavridi et al., 2005). Additionally, this region can bind to DNA in a sequence non-specific manner (Bakalkin et al., 1995, Wu et al., 1995, Ahn and Prives, 2001, Kim and Deppert, 2003). Various *in vitro* experiments have shown that this region can enhance the DBD's DNA binding affinity (Appella and Anderson, 2000, Brooks and Gu, 2003, McKinney et al., 2004, Xu, 2003). *In vivo* experiments have suggested that post-translational modifications are necessary to activate p53 transcriptional activity, and work by recruiting multiple coactivators to p53 target genes (Stavridi et al., 2005)

1.4 Efforts towards p53 structures

Although over 50,000 research papers have been published about p53, its complete three-dimensional structure remains unsolved. The main difficulty to solve the full length structure of p53 has been the inherent flexibility of unfolded regions located at both N- and C-termini (Bell et al., 2002). The structural work on p53 has focused on determining the individual domains of p53. The first published structure was the complex of p53-DBD with DNA (Cho et al., 1994). Besides the tetramerization domain already described, a structure of the N-terminus of MDM2 complexed with a short peptide of p53 TAD was solved

(Kussie et al., 1996). More recently, various structures of other proteins with fragments of the p53 regulatory domains have also been determined (Rustandi et al., 2000, Avalos et al., 2005, Lowe et al., 2002). Table 1 shows recent p53 structures that have determined through X-ray crystallography. As shown in the table, a tremendous effort has been focused on the structure of the DNA binding domain. This is mainly because 80% of human tumors have mutations in this core region (Olivier et al., 2002).

The structures of p53 DNA binding domain and tetramerization domains are well studied. More efforts need to focus on the unfolded intrinsically disordered regions formed by the transactivation domain and regulatory domain. Mutations in the transactivation domain significantly decrease the binding affinity of MDM2 and p300 for p53 (Joerger and Fersht, 2008). Additionally, mutations in the regulatory domain can affect the modulated response of p53 to cellular stresses. Eventually, this can impair DNA binding affinity, coactivator recruitment, and p53 cellular levels (Joerger and Fersht, 2008). Future structural studies should focus on understanding the crosstalk between p53 domains, and how post-translational modifications induce conformational changes in p53 that may affect its regulatory activity.

1.5 Objectives of Thesis

p53 is one of the most thoroughly studied proteins in the human genome. Extensive studies have shown that many of autoregulatory feedback loops of p53 involve MDM2, thus emphasizing the crucial role of MDM2 in the signaling pathways (Harris and Lavine, 2005). Although a variety of p53 structures have been elucidated by Nuclear Magnetic Resonance (NMR), Electron Microscopy (EM), and X-ray crystallography, the structure of p53-MDM2 complex is yet unknown.

Some clinical researches have implicated MDM2 gene amplification in certain types of tumor cells, which can lead to over-suppression of p53 transcriptional activity (Kussie et al., 1996). One way to restore the function of p53 in these cases is to develop a drug that can break the interaction between p53 and MDM2 complex.

As emphasized above, p53 and MDM2 play significant roles in the regulation of malignant cells. The structures of these two highlighted proteins provide the framework to future cancer drug development, which may target p53 mutants, MDM2 mutants, or the interaction between p53 and MDM2.

This thesis will focus on our experimental approaches to the structural studies and the biophysical characterization of two constructs: p53CTD (residue 325 to 393) and MDM2 (residue 1-491). Through this work, our ultimate goal is to understand the mechanism of p53 regulation by both its own regulatory domain and MDM2.

The overall goals of this project are:

I. To solve the structure of the p53 C-terminus domain (325 to 393) using X-ray crystallography and to study the mechanism of positive regulation of p53 DBD by the CTD

II. To examine the quaternary structure of p53CTD in the presence/absence of specific and non-specific DNA by sedimentation velocity experiments

III. To express and purify p53 variants for structural studies

IV. To study the oligomerization state of MDM2 by Transmission Electron Microscopy (TEM) and Analytical Ultracentrifugation (AUC)



Figure 1.1. **Domain Organization of Human p53**. p53 is a polypeptide of 393 amino acids. It consists of five major domains: transactivation domain (TAD), proline rich region (PRR), DNA binding domain (DBD), tetramerization domain (TD), and its regulatory domain located at its C-terminus (CT).

Table 1.1. **Recent and Highlighted p53 Structures Determination**. p53 structures were solved by X-ray crystallography.

PDB-ID	Residues	Description	Year Solved	Authors
3IGK	94-293	DNA binding domain with Hoogsteen pairs of DNA	2010	(Kitayner et al., 2010)
3KMD	92-291	DNA binding domain with 20bp DNA	2010	(Chen et al., 2010)
2WGX	96-312	DNA binding domain with mutants M133L-V203A-Y236F-N239Y-T253I-N268D	2009	(Khoo et al., 2009)
2K8F	1-39	Complex of p300 with transactivation domain	2009	(Feng et al., 2009)
3D05	94-293	DNA binding domain with mutant R249S	2009	(Suad et al., 2009)
2Z5S	17-27	Complex with MDMX with p53 binding domain	2008	(Kussie et al., 1996, Popowicz et al., 2008) (Popowicz et al., 2008)
2J1W	96-290	Mutant M133L-V143A-V203A-N239Y-N268D	2006	(Joerger et al., 2005)
2J1X	96-290	Mutant M133L-V143A-V203A-N239Y-N268D	2006	(Joerger et al., 2005)
1MA3	381-387	Acetylated K382 p53 peptide bound to Sir2Tm	2002	(Avalos et al., 2002)
IYCQ	17-27	Complex with Xenopus MDM2 p53 binding domain	1996	(Kussie et al., 1996)
IYCR	17-27	Complex with human MDM2 p53 binding domain	1996	(Kussie et al., 1996)

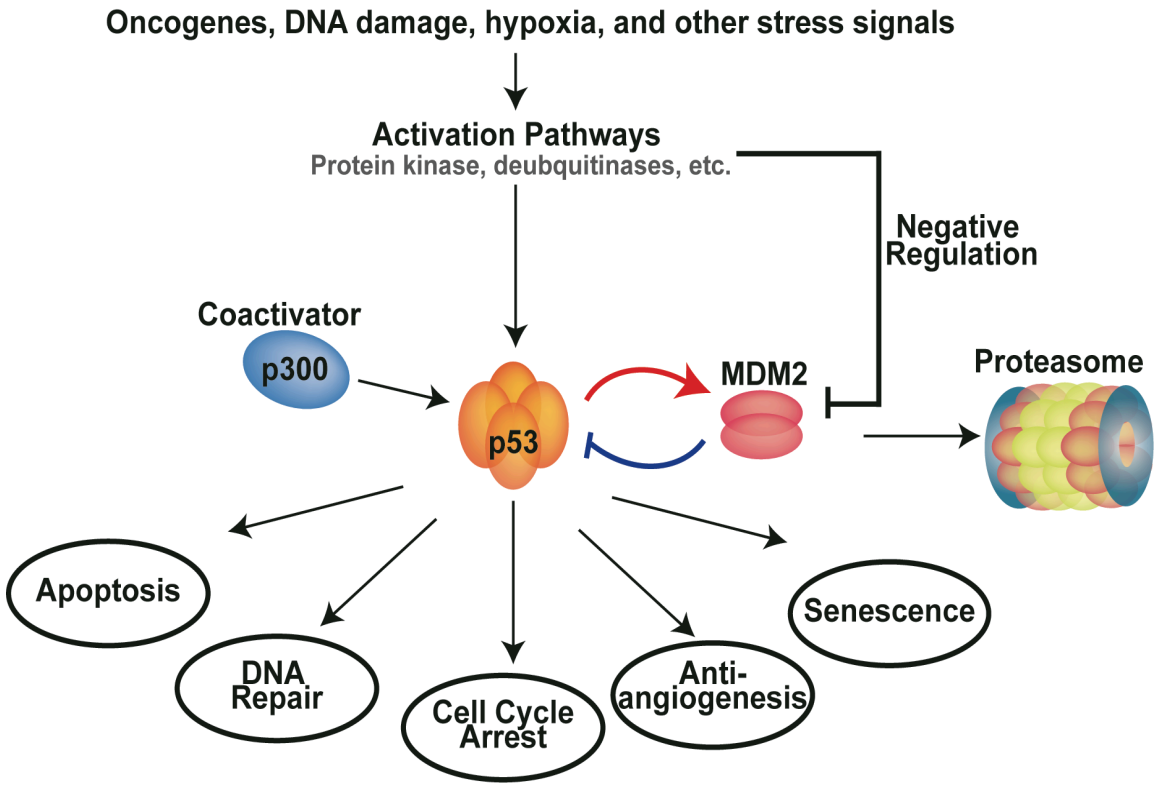


Figure 1.2. **A model of the p53 pathway**. In normal cells, p53 is negatively regulated by MDM2. MDM2 can polyubiquinate p53 for proteasomal degradation. In response to stresses, the level of p53 is increased, and promote cell to apoptosis, DNA repair, cell cycle arrest, anti-angiogenesis, and senescence.

References

AHN, J. & PRIVES, C. 2001. The C-terminus of p53: the more you learn the less you know. *Nat Struct Biol,* 8**,** 730-2.

APPELLA, E. & ANDERSON, C. W. 2000. Signaling to p53: breaking the posttranslational modification code. *Pathol Biol (Paris),* 48**,** 227-45.

AVALOS, J. L., BEVER, K. M. & WOLBERGER, C. 2005. Mechanism of sirtuin inhibition by nicotinamide: altering the NAD(+) cosubstrate specificity of a Sir2 enzyme. *Mol Cell,* 17**,** 855-68.

AVALOS, J. L., CELIC, I., MUHAMMAD, S., COSGROVE, M. S., BOEKE, J. D. & WOLBERGER, C. 2002. Structure of a Sir2 enzyme bound to an acetylated p53 peptide. *Mol Cell,* 10**,** 523-35.

BAKALKIN, G., SELIVANOVA, G., YAKOVLEVA, T., KISELEVA, E., KASHUBA, E., MAGNUSSON, K. P., SZEKELY, L., KLEIN, G., TERENIUS, L. & WIMAN, K. G. 1995. p53 binds single-stranded DNA ends through the C-terminal domain and internal DNA segments via the middle domain. *Nucleic Acids Res,* 23**,** 362-9.

BARGONETTI, J., FRIEDMAN, P. N., KERN, S. E., VOGELSTEIN, B. & PRIVES, C. 1991. Wild-type but not mutant p53 immunopurified proteins bind to sequences adjacent to the SV40 origin of replication. *Cell,* 65**,** 1083-91.

BELL, S., KLEIN, C., MULLER, L., HANSEN, S. & BUCHNER, J. 2002. p53 contains large unstructured regions in its native state. *J Mol Biol,* 322**,** 917-27.

BROOKS, C. L. & GU, W. 2003. Ubiquitination, phosphorylation and acetylation: the molecular basis for p53 regulation. *Curr Opin Cell Biol,* 15**,** 164-71.

BROWN, C. J., LAIN, S., VERMA, C. S., FERSHT, A. R. & LANE, D. P. 2009. Awakening guardian angels: drugging the p53 pathway. *Nat Rev Cancer,* 9**,** 862-73.

CHEN, Y., DEY, R. & CHEN, L. 2010. Crystal structure of the p53 core domain bound to a full consensus site as a self-assembled tetramer. *Structure,* 18**,** 246-56.

CHO, Y., GORINA, S., JEFFREY, P. D. & PAVLETICH, N. P. 1994. Crystal structure of a p53 tumor suppressor-DNA complex: understanding tumorigenic mutations. *Science,* 265**,** 346-55.

FENG, H., JENKINS, L. M., DURELL, S. R., HAYASHI, R., MAZUR, S. J., CHERRY, S., TROPEA, J. E., MILLER, M., WLODAWER, A., APPELLA, E. & BAI, Y. 2009. Structural basis for p300 Taz2-p53 TAD1 binding and modulation by phosphorylation. *Structure,* 17**,** 202-10.

GATZ, S. A. & WIESMULLER, L. 2006. p53 in recombination and repair. *Cell Death Differ,* 13**,** 1003-16.

ITAHANA, K., MAO, H., JIN, A., ITAHANA, Y., CLEGG, H. V., LINDSTROM, M. S., BHAT, K. P., GODFREY, V. L., EVAN, G. I. & ZHANG, Y. 2007. Targeted inactivation of Mdm2 RING finger E3 ubiquitin ligase activity in the mouse reveals mechanistic insights into p53 regulation. *Cancer Cell,* 12**,** 355-66.

ITAHANA, Y., KE, H. & ZHANG, Y. 2009. p53 Oligomerization is essential for its C-terminal lysine acetylation. *J Biol Chem,* 284**,** 5158-64.

JEFFREY, P. D., GORINA, S. & PAVLETICH, N. P. 1995. Crystal structure of the tetramerization domain of the p53 tumor suppressor at 1.7 angstroms. *Science,* 267**,** 1498-502.

JOERGER, A. C., ANG, H. C., VEPRINTSEV, D. B., BLAIR, C. M. & FERSHT, A. R. 2005. Structures of p53 cancer mutants and mechanism of rescue by second-site suppressor mutations. *J Biol Chem,* 280**,** 16030-7.

JOERGER, A. C. & FERSHT, A. R. 2008. Structural biology of the tumor suppressor p53. *Annu Rev Biochem,* 77**,** 557-82.

KHOO, K. H., JOERGER, A. C., FREUND, S. M. & FERSHT, A. R. 2009. Stabilising the DNA-binding domain of p53 by rational design of its hydrophobic core. *Protein Eng Des Sel,* 22**,** 421-30.

KIM, E. & DEPPERT, W. 2003. The complex interactions of p53 with target DNA: we learn as we go. *Biochem Cell Biol,* 81**,** 141-50.

KITAYNER, M., ROZENBERG, H., ROHS, R., SUAD, O., RABINOVICH, D., HONIG, B. & SHAKKED, Z. 2010. Diversity in DNA recognition by p53 revealed by crystal structures with Hoogsteen base pairs. *Nat Struct Mol Biol,* 17**,** 423-9.

KUSSIE, P. H., GORINA, S., MARECHAL, V., ELENBAAS, B., MOREAU, J., LEVINE, A. J. & PAVLETICH, N. P. 1996. Structure of the MDM2 oncoprotein bound to the p53 tumor suppressor transactivation domain. *Science,* 274**,** 948-53.

LAVIN, M. F. & GUEVEN, N. 2006. The complexity of p53 stabilization and activation. *Cell Death Differ,* 13**,** 941-50.

LOWE, E. D., TEWS, I., CHENG, K. Y., BROWN, N. R., GUL, S., NOBLE, M. E., GAMBLIN, S. J. & JOHNSON, L. N. 2002. Specificity determinants of recruitment peptides bound to phospho-CDK2/cyclin A. *Biochemistry,* 41**,** 15625-34.

MCKINNEY, K., MATTIA, M., GOTTIFREDI, V. & PRIVES, C. 2004. p53 linear diffusion along DNA requires its C terminus. *Mol Cell,* 16**,** 413-24.

OLIVIER, M., EELES, R., HOLLSTEIN, M., KHAN, M. A., HARRIS, C. C. & HAINAUT, P. 2002. The IARC TP53 database: new online mutation analysis and recommendations to users. *Hum Mutat,* 19**,** 607-14.

OREN, M. 2003. Decision making by p53: life, death and cancer. *Cell Death Differ,* 10**,** 431-42.

PAVLETICH, N. P., CHAMBERS, K. A. & PABO, C. O. 1993. The DNA-binding domain of p53 contains the four conserved regions and the major mutation hot spots. *Genes Dev,* 7**,** 2556-64.

POPOWICZ, G. M., CZARNA, A. & HOLAK, T. A. 2008. Structure of the human Mdmx protein bound to the p53 tumor suppressor transactivation domain. *Cell Cycle,* 7**,** 2441-3.

RUSTANDI, R. R., BALDISSERI, D. M. & WEBER, D. J. 2000. Structure of the negative regulatory domain of p53 bound to S100B(betabeta). *Nat Struct Biol,* 7**,** 570-4.

STAVRIDI, E. S., HUYEN, Y., SHESTON, E. A. & HALAZONETIS, T. D. 2005. The Three-Dimensional Structure of p53. *The p53 Tumor Suppressor Pathway and Cancer,* 2**,** 25-52.

STAVRIDI, E. S., HUYEN, Y., SHESTON, E.A. AND HALAZONETIS, T.D. 2005. The Three-Dimensional Structure of p53. *The p53 Tumor Suppressor Pathway and Cancer,* 2.

SUAD, O., ROZENBERG, H., BROSH, R., DISKIN-POSNER, Y., KESSLER, N., SHIMON, L. J., FROLOW, F., LIRAN, A., ROTTER, V. & SHAKKED, Z. 2009. Structural basis of restoring sequence-specific DNA binding and transactivation to mutant p53 by suppressor mutations. *J Mol Biol,* 385**,** 249-65.

TOLEDO, F. & WAHL, G. M. 2006. Regulating the p53 pathway: in vitro hypotheses, in vivo veritas. *Nat Rev Cancer,* 6**,** 909-23.

VIADIU, H. 2008. Molecular architecture of tumor suppressor p53. *Curr Top Med Chem,* 8**,** 1327-34.

VOGELSTEIN, B., LANE, D. & LEVINE, A. J. 2000. Surfing the p53 network. *Nature,* 408**,** 307-10.

WU, W. J., KAKEHI, Y., HABUCHI, T., KINOSHITA, H., OGAWA, O., TERACHI, T., HUANG, C. H., CHIANG, C. P. & YOSHIDA, O. 1995. Allelic frequency of p53 gene codon 72 polymorphism in urologic cancers. *Jpn J Cancer Res,* 86**,** 730-6.

XU, Y. 2003. Regulation of p53 responses by post-translational modifications. *Cell Death Differ,* 10**,** 400-3.

Chapter Two

Structural Studies and Biophysical Characterization of p53CTD

Introduction

When DNA is damaged or otherwise cells undergo stress, activation of the p53 tumor suppressor protein protects the integrity of the genome by inducing, DNA repair, cell cycle arrest and apoptosis (May and May, 1999, Vogelstein et al., 2000, Hupp et al., 2000). Activation of tumor suppressor activity requires p53 to be in a tetrameric state, which is mediated by the tetramerization domain near its C-terminus. When p53 is in its oligomeric form, it is able to bind to the twenty base pair DNA consensus sequences via its central DNA binding domain (Sakamoto et al., 1994, Wang et al., 1994).

It has been shown that in addition to the specific DNA binding mediated by the DNA binding domain, interactions of p53 with a wide variety of DNA structures can also be mediated by the regulatory domain (Ahn and Prives, 2001). This is a distinct feature of p53. The real biological function of the regulatory domain of p53 is still not completely clear. An *in vitro* study where linear diffusion of p53 on DNA is measured shows that p53 lacking the regulatory domain has a lower DNA affinity, suggesting that the regulatory domain can positively regulate the affinity of the DNA binding domain (McKinney et al., 2004). However, there is a lack of structural information about how such regulation might be occurring.

Numerous structures of p53 DNA binding domain in complex with DNA have been solved through high-resolution X-ray crystallography, as well as isolated p53 tetramerization domain (Chen et al., 2010, Cho et al., 1994, Jeffrey et al., 1995). The tetramerization domain has been particularly well studied

because each thirty amino acids monomer contributes a β-strand and an α-helix to form a dimer of dimers kept together by a hydrophobic core. Furthermore, the tetramerization domain does not require any metals or prosthetic groups to fold (Clore et al., 1994, Jeffrey et al., 1995, McCoy et al., 1997). In contrast, the structure of the regulatory domain of p53 is still undetermined due to difficulties in crystallizing this intrinsically unfolded, flexible region (Bell et al., 2002). The inherent flexibility of the regulatory domain of p53 is one of the main reasons why the structure of full-length p53 has still not been determined. To understand the three-dimensional structure of full length p53 would help us to decipher its complex biological. Our present effort aims to bring us closer to such goal.

Since mutations in p53 are implicated in 50% of human cancers, p53 has the potential to become an important target for the development of anti-cancer drugs. In this thesis, we initially focused on using X-ray crystallography to elucidate the molecular structure of p53CTD, which contains the tetramerization domain and the regulatory domain (Figure 2.1). In addition to the structural studies, we also carried out biophysical experiments to gain insight on how the p53CTD behaves in the presence of DNA.

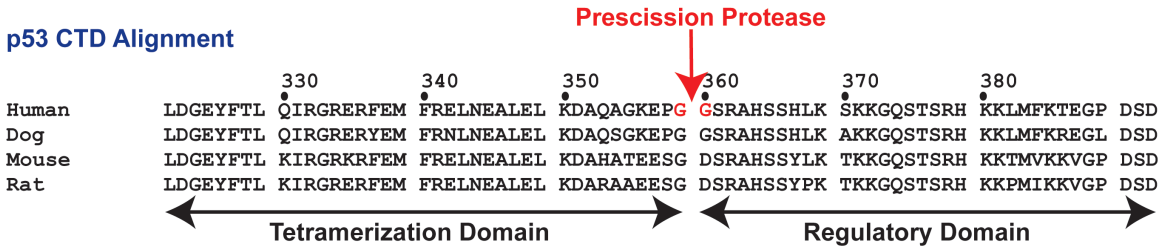


Figure 2.1. **Domain organization and sequence of p53CTD**. p53CTD is a polypeptide chain of 70 amino acids from residues 323 to 393. It consists of two domains: the tetramerization domain and the regulatory domain. The peptide bond between Gly360 and Gly361 was cleaved by PreScission protease during crystallization.

Materials and Methods

Cloning

The DNA sequence encoding the amino acid residues from 323 to 393 of human p53 (p53CTD) was PCR amplified using designed primers that annealed to the full-length p53 gene. The amplified DNA fragment was cloned into the pMal-p2G expression vector (Biolabs) using *Eco*RI and *Hind*III as cloning sites. In this construct the maltose binding protein (MBP) tag can be separated from p53CTD by the specific Prescission protease cleavage between the Gln and Gly residues of the recognition sequence of LeuGluValLeuPheGln/GlyPro. The cloned plasmid was sequenced and then transformed into *E. coli* BL21(DE3) (Stratagene)

Expression

To express p53CTD in bacteria, an overnight culture of 5 mL of Luria–Bertani (LB) and 100 μg/ml of ampicillin was transferred into 1 L of LB medium and further cultured at 37 °C until the OD_{600} reached about 0.6. Protein expression was carried for 4 hours at 25 °C and induced by the addition of 0.5 mM isopropyl-b-D-thiogalactopyranoside (IPTG).

Purification

Cells expressing p53CTD were harvested by centrifugation at 4,250 r.p.m. for 20 minutes and the bacterial pellets were resuspended in a buffer containing 150 mM NaCl, 50 mM Tris-HCl (pH 7.0) and 0.04 mM phenyl-

methanesulfonylfluoride (PMSF protease inhibitor). Cells were lysed by French press, the lysate was cleared by ultracentrifugation at 30,000 r.p.m. and the recombinant fusion protein was purified by affinity chromatography using 1 mL of amylose resin. The amylose-bound fusion protein (MBP-pp-p53CTD) was transferred to a gravity column and washed with 100 mL of low salt buffer. After washing, the protein was eluted by adding 50 mM maltose to the buffer. PreScission Protease (8 μg per 1mg of protein) was added to the elution and left for overnight digestion at 4 °C (Figure 2.2). After cleavage of the fusion protein with PreScission Protease, further purification took advantage of isoelectric point differences between p53CTD (p*I*: 8.35, MW 8.2 kDa) and MBP (p*I*: 5.07, MW: 42.5 kDa) with SP-Sepharose cation-exchange chromatography. The Mono-S column was equilibrated with 150 mM NaCl, 50 mM Tris HCl at pH 7.0 buffer to enable p53CTD to bind to the column; the maltose binding protein (MBP) eluted in the unbound fractions. The column was washed with 50ml of binding buffer, and p53CTD was eluted using 1 M NaCl (Figure 2.2). The purified protein was desalted (50 mM NaCl, 25 mM Tris HCl, and pH 7.0) using a gel filtration column Sephadex G25 (Figure 2.3). SDS–PAGE (15%, w/v) and MALDI-TOF analysis were done to evaluate the purity of the sample (Figure 2.5).

Crystallization

The protein was concentrated to 10 mg/mL, and crystallization was carried out via the hanging-drop vapor-diffusion method at 20 °C using VDX multiwell plates (Hampton). Preliminary screenings were performed using the Hampton, PEG/Ion

Screen kit. Small crystals appeared in the reservoir solution consisting of 150 mM calcium acetate and 12% polyethylene glycol 3350 (PEG 3350). After optimization, bigger crystals were obtained at 20 degrees from a reservoir solution containing 80 mM calcium acetate, 18% (w/v) PEG 3350 and 10% glycerol. Crystals suitable for X-ray data collection appeared within 14 days and reached final dimensions of 1.0 x 0.4 x 0.1 mm (Figure 2.7). Selenomethionine labeled p53CTD was expressed using a previously published protocol (Van Duyne et al., 1993). It was purified and crystallized using the same protocol used for the unlabeled construct.

X-ray intensity data collection and processing

Crystal structure determination was carried by postdoctoral fellow Abdul Ethayathulla. X-ray intensity data collection was done at the Stanford Synchrotron Radiation Laboratory (SSRL). Diffraction data were collected using an ADSC Quantum-315R CCD detector on the BL7-1 beamline. The crystals were flash-cooled in a nitrogen gas stream at 100 °K using 20%(v/v) PEG 400 as a cryoprotectant in a drop made up of equal volumes of the protein solution and reservoir solution containing 0.15 M calcium acetate, 20%(w/v) PEG 3350, and 10% glycerol). Crystals were maintained at 100 °K during data collection. The crystal-to-detector distance was set to 200 mm. A MAD (multiple anomalous dispersion) data set was collected corresponding to the maximum f''(peak, 0.9762 Å), the minimum f' (edge, 0.9797 Å) and a reference wavelength (remote, 0.9716 Å) chosen on the basis of the absorption spectrum of the Se atom. The

diffraction data were processed with the HKL 2000 package (Otwinowski and Minor, 1997) (Figure 2.8). The crystallographic data and the MAD data statistics are summarized in Table 1. The hexagonal crystals belong to the space group $P6_522$ with unit cell parameters a = b = 49.603 Å, c = 92.95 Å, γ = 120.0°. Assuming the presence of one molecule (72 amino acid residues) in the asymmetric unit, the calculated VM is 2.84 $Å^3$/Da, which corresponds to a solvent content of 56.6% (Matthews, 1968). A high-quality diffraction data set was obtained to 2.30 Å resolution, with 100% completeness and an R_{merge} of 6.0% (Table 2.1). Although crystal structure of p53 tetramerization domain (323-353) (PDB ID: 1C26) was known, we were not able to phase our data using the molecular replacement method. We were able to calculate initial phases by the MAD method. The 2 expected SeMet sites in the structure were found with the program SOLVE (Terwilliger and Berendzen, 1999) and these peaks were further refined using RESOLVE (Terwilliger, 2000, Terwilliger, 2003). Using the PHENIX automated crystallographic program (Adams et al., 2002, Murshudov et al., 1997), the structure was solved with R_{cryst}/R_{free} = 0.32/0.38, and the structure was found to be a dimer of the p53 tetramerization domain (323-353), each containing one SeMet site. Although the structure is similar to that of a previously solved structure we were not able to solve it via the molecular replacement method. The structure was further refined and omit-maps were calculated in order to check whether we could see the density for the regulatory domain (354-393). The unit cell packing showed that we were able to crystallize only the p53 tetramerization domain (323-353) (Figure 2.9). In order to confirm whether the

regulatory domain of p53CTD was cleaved, crystals of p53CTD were washed twice and dissolved in de-ionized water. The MALDI analysis of the crystal was done using MALDI-TOF. The mass spectrum of the dissolved crystals showed two peaks, compared with one peak in the MALDI spectrum of p53CTD prior to crystallization (Figure 2.6). This result showed that p53CTD was cleaved into two fragments, suggesting that p53CTD was subject to proteolysis during crystallization and explaining why we were only able to crystallize the tetramerization domain in absence of the regulatory domain.

The structure of p53CTD (323-353) was further refined with the programs suite REFMAC 5.0 (Murshudov et al., 1997). Several further rounds of refinement with REFMAC 5.0 (Murshudov *et al*., 1997) interspersed with model building using $|2F_o - F_c|$ and $|F_o - F_c|$ Fourier maps (Figure 2.10) converged the refinement to R_{cryst} and R_{free} factors of 0.236 and 0.28, respectively. The refinement calculations were interleaved with several rounds of model building with the program coot (Emsley et al., 2010). The refinement statistics are shown in Table 2.1.

Analytical Ultracentrifugation (AUC)

A 400μL aliquot of a protein-DNA complex solution containing 0.15 mg of protein and 10.5 μg of DNA in 100 mM NaCl, 20 mM Na_2HPO_4, pH 7.0 buffer were used for the experiments carried out at 20°C in a Beckman Optima-XL-I analytical ultracentrifuge. Protein-DNA complex (400μL) and buffer (400μL) were loaded into a double-sector centerpiece. The cells were loaded into an AN56Ti

analytical rotor and accelerated to 50,000 rpm. Scans were acquired in continuous mode at 260nm for DNA and 488nm for fluorescein-labeled DNA in the range of 0.1 to 1 absorption units. The collected data were analyzed using the program SEDFIT fitting the Lamm Equation using a c(S) distribution model (Lebowitz et al., 2002). The partial specific volume, buffer viscosity, and buffer density were calculated against 100 mM sodium chloride, 20 mM Na_2HPO_4, and pH 7.0 through SEDNTERP (Laue et al., 1992).

Table 2.1. **Data Collection Table of p53CTD crystal**.

Data Collection	Peak	Inflection	remote
Wavelength (Å)	0.9764	0.9797	0.9716
Resolution (Å)	100 – 2.3	100 – 2.3	100 – 2.3
Space group	$P6_522$	$P6_522$	$P6_522$
Cell dimensions (Å)	a=b= 49.6, c=92.5	a=b= 49.6, c=92.5	a=b= 49.6, c=92.5
Unique reflections	5723	5728	5734
R_{sym} (%)	6.0(39)	7.0(47)	7.6(46)
I/σ (I)	28.6(5.2)	29.0(4.5)	26.2(3.4)
Completeness (%)	97.3(93.4)	97.4(93.0)	99.9(100)
Redundancy	11.0	10.8	10.6
Refinement			
R_{work}/R_{free}	0.23/0.28		
Protein	566		
B-factors ($Å^2$)	40.2		
Rms deviations			
Bond length (Å)	0.004		
Bond angles (°)	0.59		

Results

Overall structure of p53CTD (323-353)

The overall fold of p53CTD (323-353) is similar to the previously solved structures 1C26 and 1ALE (Jeffrey et al., 1995). The overall structure consists of two homo-dimers, with each monomer containing 30 amino acid (Figure 2.11). Each monomer consists of one β-strand from residue 326 to 333 followed by an α-helix from residues 335 to 354. The α-helix and the β-strand form a V-shaped structure with Gly334 as the hinge residue. Dimerization occurs such that the β-strands are anti-parallel and the α-helices cross below it. The tetramer is effectively a dimer of dimers in which the AB and CD dimers interact via the α-helices (Figure 2.12). In each monomer, a small hydrophobic core consisting of the buried side chains Ile332 and Phe341 and the partially buried side chains Phe338 and Leu330 was observed. Our crystal structures also agreed with the observation of an intermonomer salt link between Arg337 and Asp352 and an intermonomer hydrogen bond between Try327 and Arg333 (Jeffrey et al., 1995). In the dimer-dimer (AB & CD) interaction, hydrophobic interactions were observed between three buried side chains: Ala347, Phe341, and Leu344 (Figure 2.13).

p53CTD mutant G360S and G361A

Based on the fragments we observed from the mass spectrometry spectrum of the p53CTD dissolved crystal, we designed a double p53CTD mutant G360S and G361A aiming to prevent the proteolysis that occurred during

crystallization (Figure 2.6). The site between Gly360 and Gly361 was identified as the non-specific cleavage site for PreScission Protease. The p53CTD G360S/G361A double mutant was purified following the same protocol as p53CTD (Figure 2.14). However, the fusion protein was not cleaved completely and several impurities were observed in SDS-PAGE analysis (Figure 2.15). Circular dichroism experiments showed different secondary structure composition for the mutant and we did not continue studying it.

In addition to studying the structure of p53CTD, we were also interested in characterizing the DNA-induced changes on the quaternary structure of p53CTD. Therefore, the protein was purified again using the unlabeled construct, and DNA binding studies were carried out using analytical ultracentrifugation (AUC). This method was chosen because of its sensitivity to molecular weight differences. From the sedimentation coefficients obtained from AUC, we were able to calculate the molecular weight, and hence the dimerization state of p53CTD in the presence of DNA. In the sedimentation velocity experiments, we used 4 different sets of DNA complexed with p53CTD (Table 3.2).

DNA binding studies using analytical ultracentrifugation

Based on previous biochemical and structural studies of the p53 DNA binding domain with various consensus DNA sequences. We chose three sequences of varying length to study the DNA binding properties of p53CTD. Three 5'-fluorescent labeled oligos: (1) 14 bp 5'-ATGGACATGTCCAT-3', (2) 14 bp 5'-TGCCCGTACGGGCA-3' and (3) 24 bp-5'-TCGGGCATGCCCGG-

GCATGCCCGA-3' were made (IDT). The oligonucleotides were dissolved in a buffer containing 100mM NaCl, 20mM Na_2HPO_4, pH 7.0 to achieve a concentration of approximately 815 mg/mL. Synthesized double stranded oligonucleotides were annealed at 100°C for 3 minutes and cooled down slowly to room temperature for an hour.

p53CTD is in its dimeric state in the presence of the DNA consensus sequence

In order to study the interaction of p53CTD and DNA by sedimentation velocity, it is first necessary to determine the sedimentation coefficient of each partner independently in the experimental conditions. Moreover, since the experimentally sedimentation coefficient vary with temperature and buffer density, we converted it into a standard state against water at 20 ºC. Figure 2.16 represents sedimentation distribution of p53CTD alone monitored at 280nm. The distribution shows one peak centered at an apparent sedimentation coefficient of 2.25. This indicates the presence of p53 in its tetrameric state with an experimental molecular weight of 34.7 kDa, which is closed to the theoretical molecular weight of p53CTD (32.7 kDa). The p53 tetramer peak accounts for 78.50% of the sample.

Figure 2.17 represents the sedimentation distribution of p53CTD in complex with the 14 b.p. DNA sequence previously used to crystallize the p53 DNA binding domain (Jeffrey et al., 1995). Three peaks were shown in the analysis. In this experiment, 6.31% of sample was shown to be dimeric p53CTD

complexed with the 14 bp DNA sequence, suggesting that p53CTD could also recognize the DNA that originally binds to the p53 DNA binding domain (Table 2.3).

p53CTD is in its dimeric state in the presence of non-specific DNA sequences

The regulatory domain of p53 is known to bind to a wide variety of DNA structures in a non-specific manner (McKinney et al., 2004). We carried out experiments is to examine the interaction between p53CTD and non-specific DNA sequences. We designed a non-specific fluorescein-labeled 14 bp DNA sequence (Table 2.2). In the analysis of this experiment, we obtained a profile that was similar to our previous experiment with specific DNA (Figure 2.18). As shown, about 30% of sample was present as dimeric p53CTD complexed with the non-specific p53 14 bp fluorescein DNA (Table 2.4). This experiment supports the hypothesis that the regulatory domain of p53 can bind to DNA in a non-specific sequence manner.

p53CTD is in its dimeric state in the presence of non-specific DNA sequences regardless of length

Our next goal was to examine the interaction of p53CTD with a DNA of different length. In this experiment, we designed a fluorescein-labeled 24 bp DNA sequence (Table 2.2). As expected, the same sedimentation profile was obtained as in previous experiments (Figure 2.19). It is interesting to note that a higher

percentage of dimeric p53CTD in complex with the DNA was seen in the sample (Table 2.5). This result confirms the hypothesis that p53CTD can bind to non-specific DNA sequences regardless of DNA length.

Summary of p53CTD-DNA binding studies

The sedimentation distribution experimental results indicate that p53CTD changes from a tetrameric state in solution to a dimeric state in the presence of DNA, regardless of DNA sequence and length.

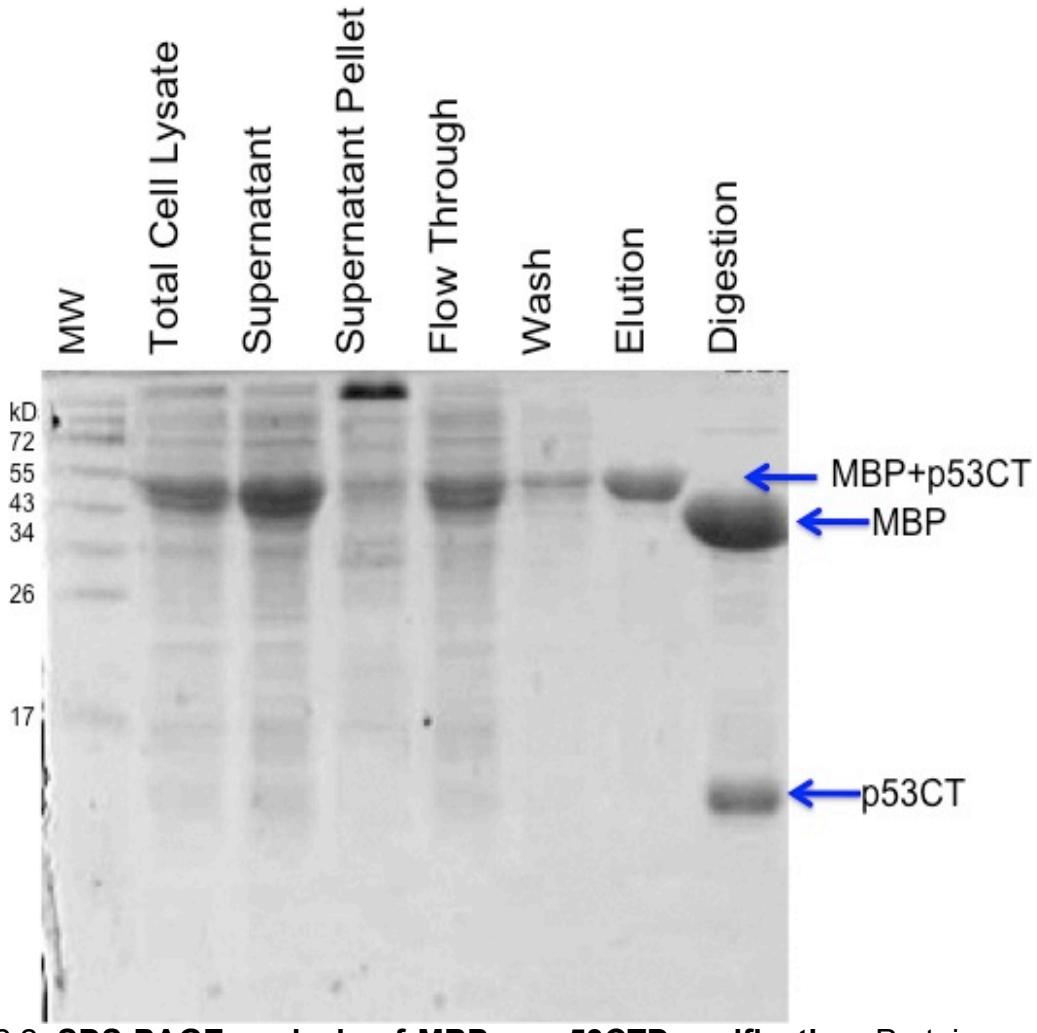


Figure 2.2. **SDS-PAGE analysis of MBP-pp-p53CTD purification**. Protein was eluted from the affinity column with a solution of 50mM maltose and runs with an apparent M.W. of around 50 kDa on SDS-PAGE. Eluted protein was digested overnight with PreScission Protease. After cleavage, two fragments were shown: Maltose binding protein (40 kDa) and p53CT (8kDa).

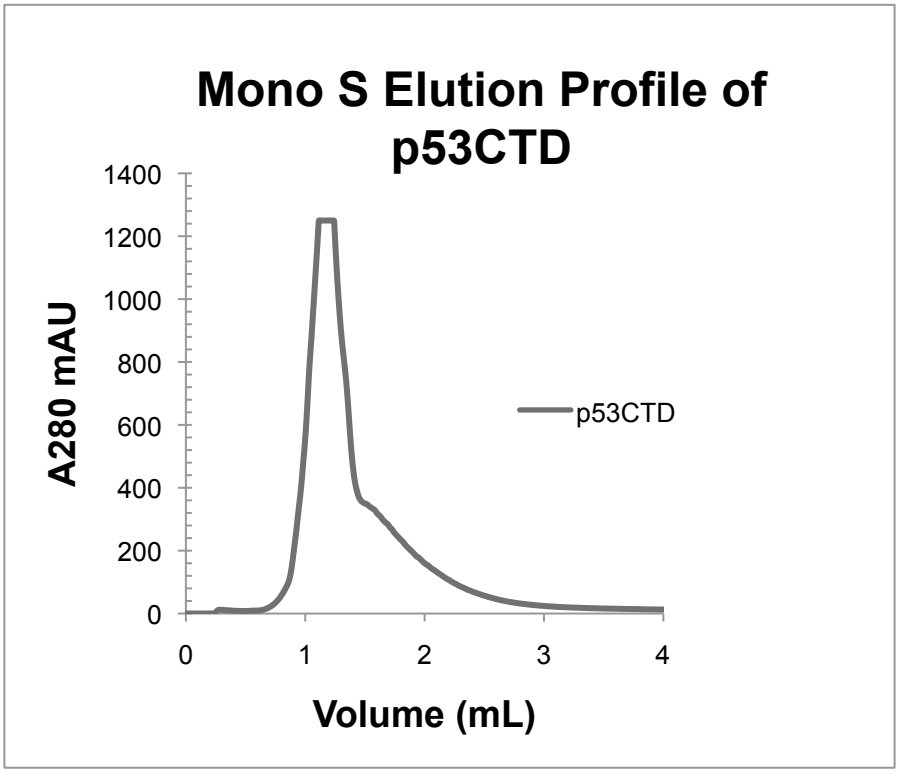


Figure 2.3. **MonoS Elution Profile of p53CTD.** A single peak was observed from the chromatogram in buffer B (1M NaCl, 50mM Tris HCl, pH 7.0).

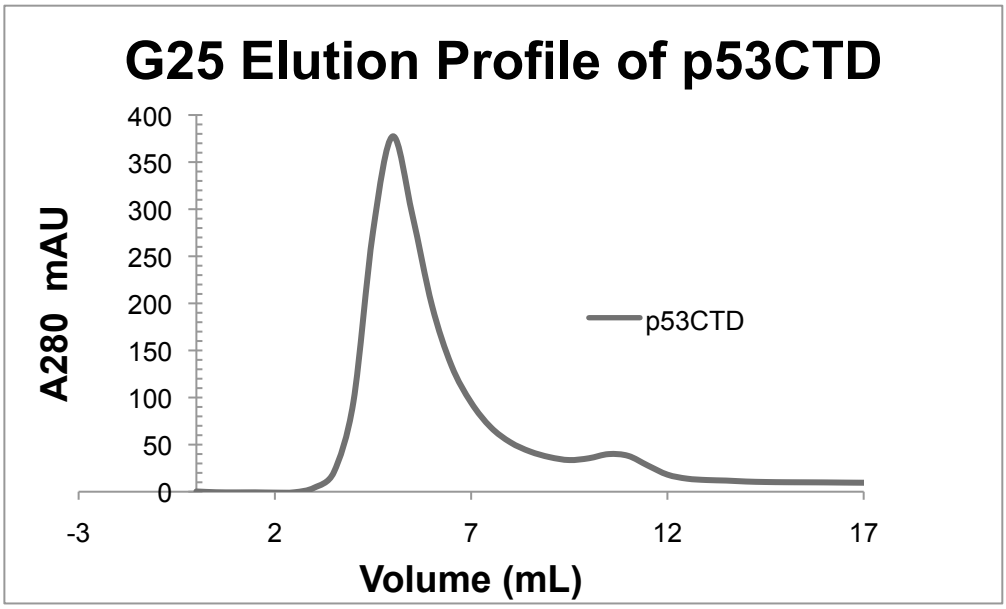


Figure 2.4. **Gel filtration profile of p53CTD using G25.** p53CTD was desalted in a buffer containing 50mM NaCl, 25mM Tris HCl, pH 7.0 and used for protein crystallization.

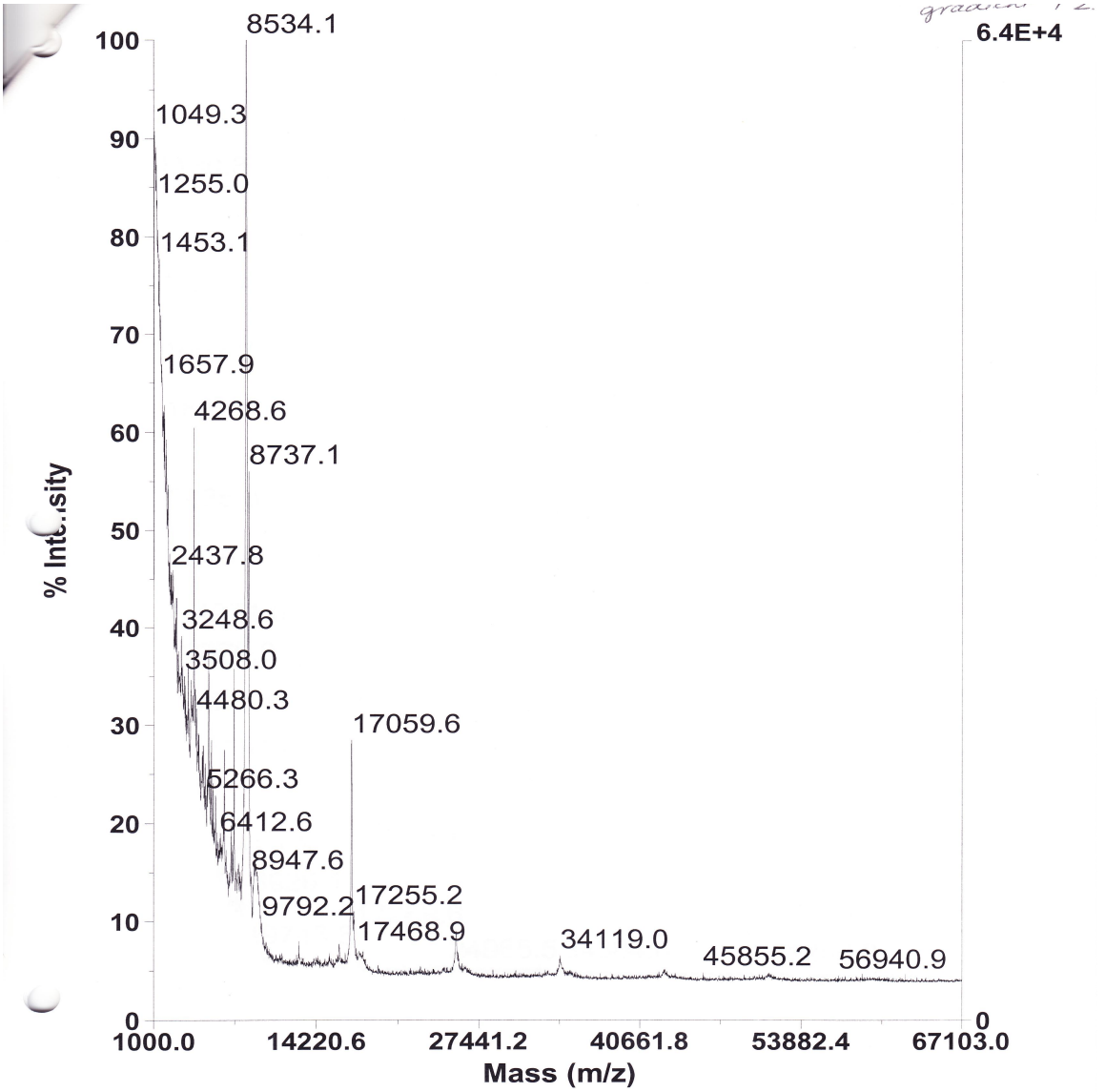


Figure 2.5. **MALDI-TOF Spectrum of SeMeth p53CTD before crystallization**. The experimental molecular weight of 8534.1 Da is close to the theoretical molecular weight of 8542.5 Da.

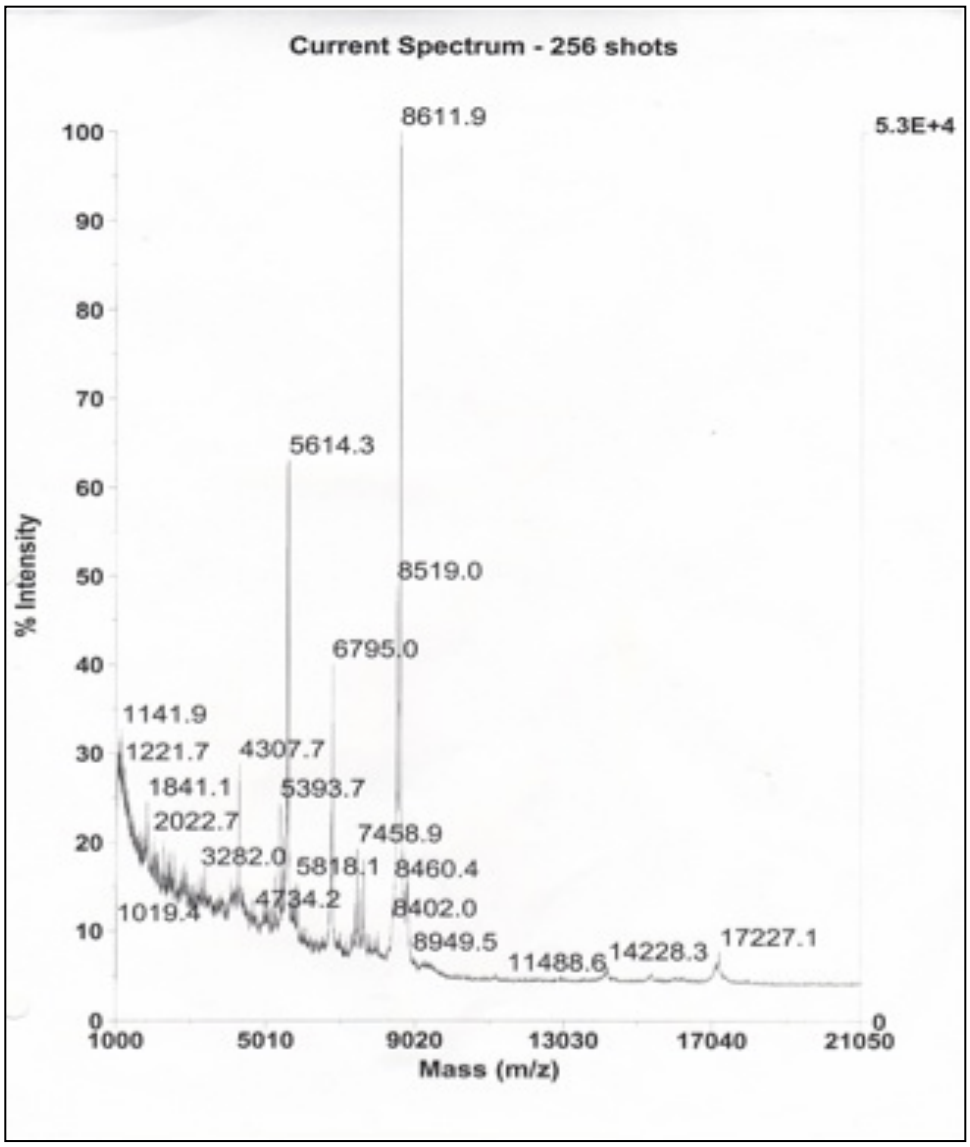


Figure 2.6. **MALDI-TOF spectrum of SeMet p53CTD dissolved crystal.** It has a high intensity peak of 8527.2 Da corresponding to the intact p53CTD protein construct and two peaks at 5614.3 Da and 6795.0 Da corresponding to the digested fragments.

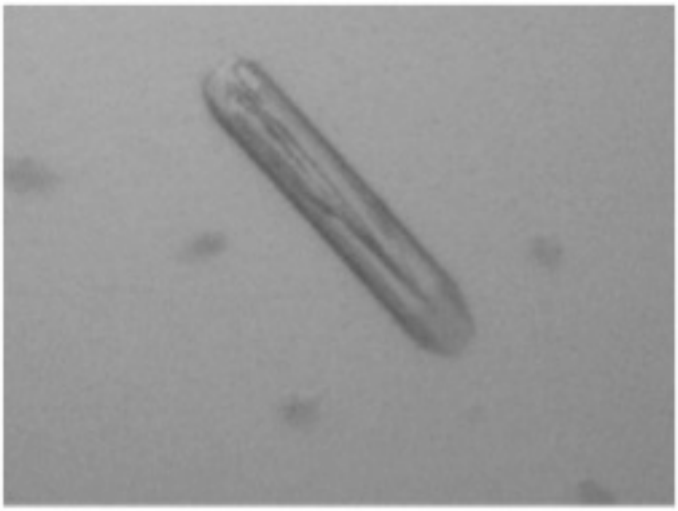


Figure 2.7. **p53CTD crystal**. The crystal of p53CTD was rod-shaped and belongs to the hexagonal space group $P6_522$.

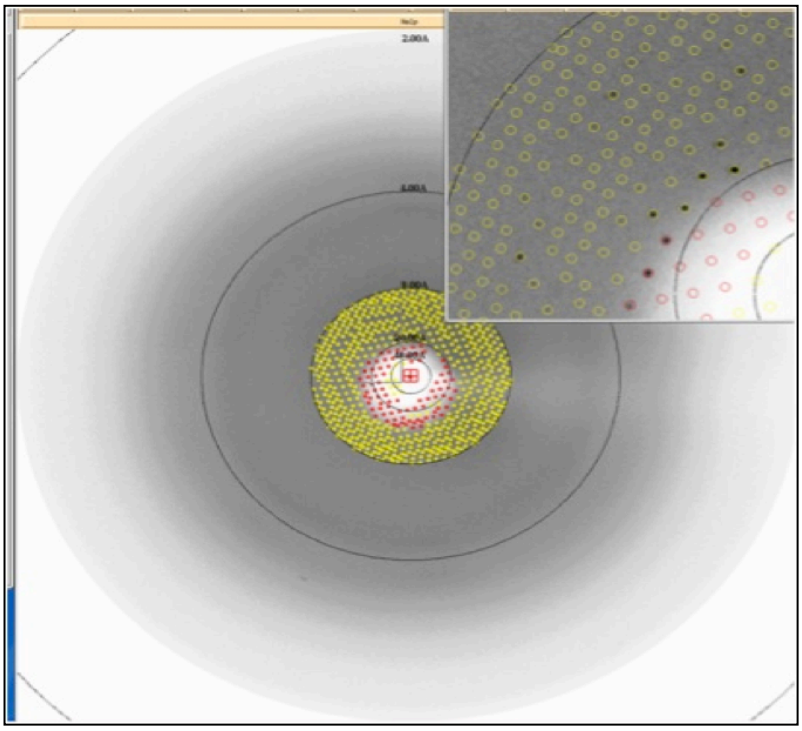


Figure 2.8. **One degree oscillation diffraction pattern of p53CTD crystal collected at SSRL BL7-1.** The crystal diffracted to 2.3 Å.

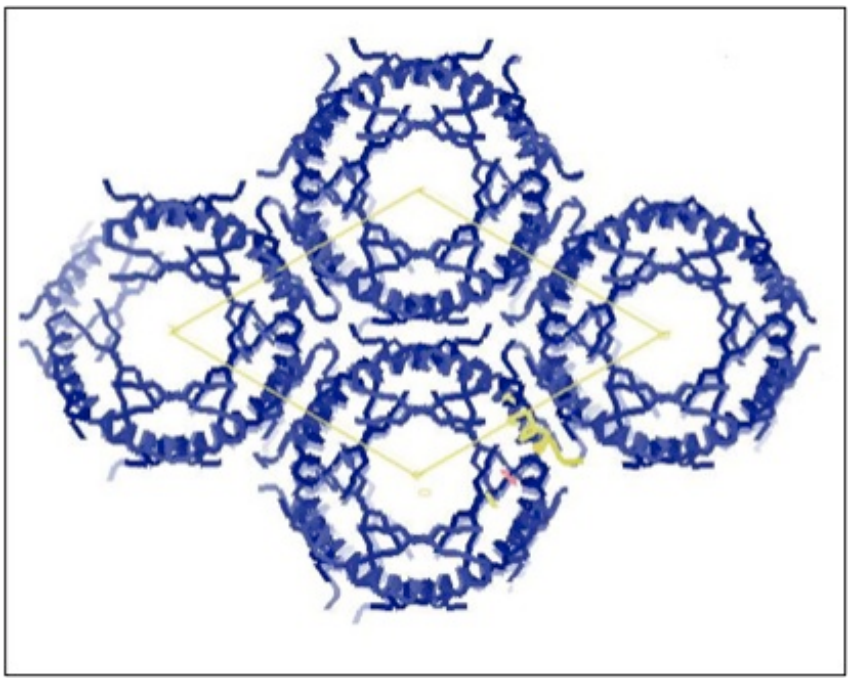


Figure 2.9. **Crystal packing of p53CTD**.

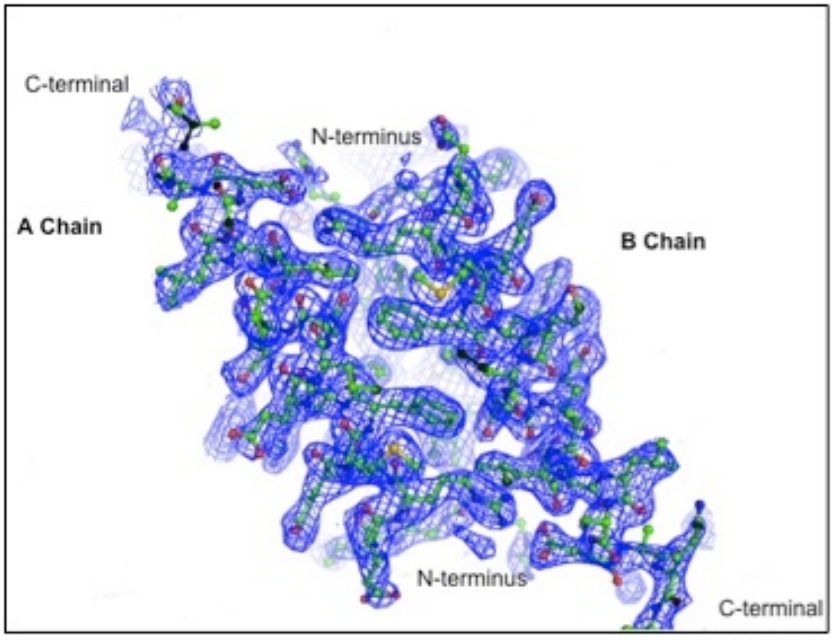


Figure 2.10. **$|2F_o\text{-}F_c|$electron density map of p53CTD dimer**.

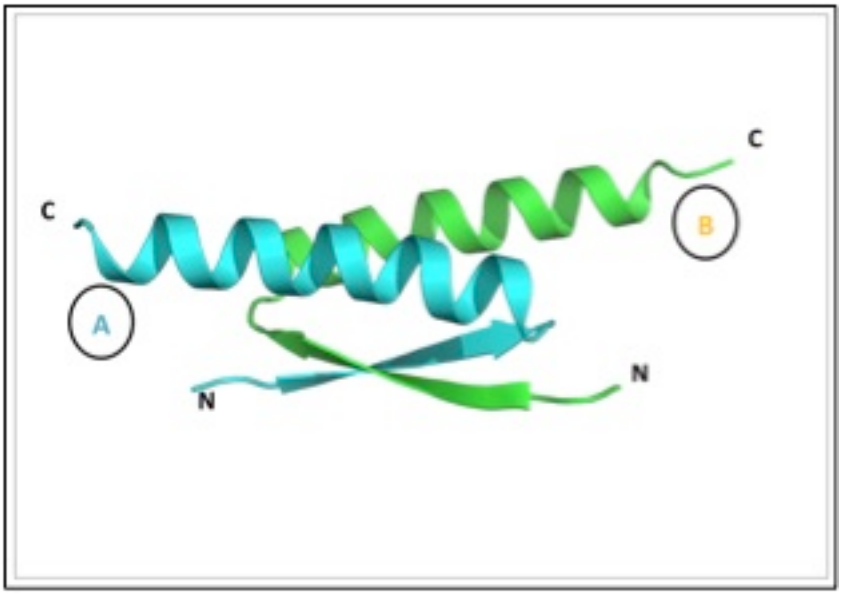


Figure 2.11. **Dimer of p53CTD observed in the unit cell**.

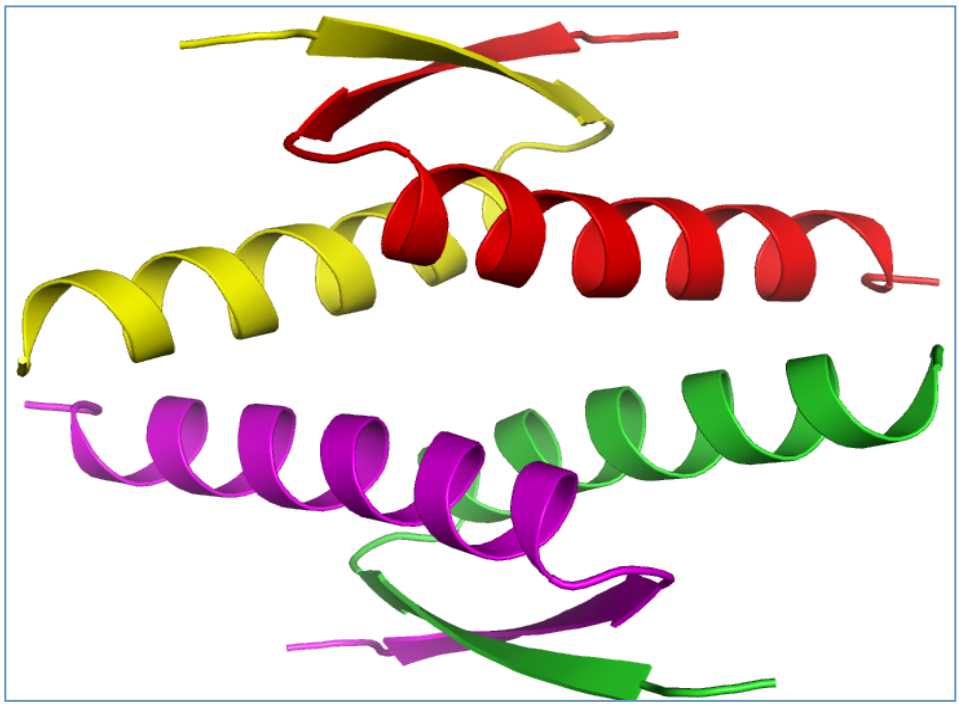


Figure 2.12. **Tetramerized state of p53CTD**. The tetramerization is composed of dimers of symmetry-related homodimers.

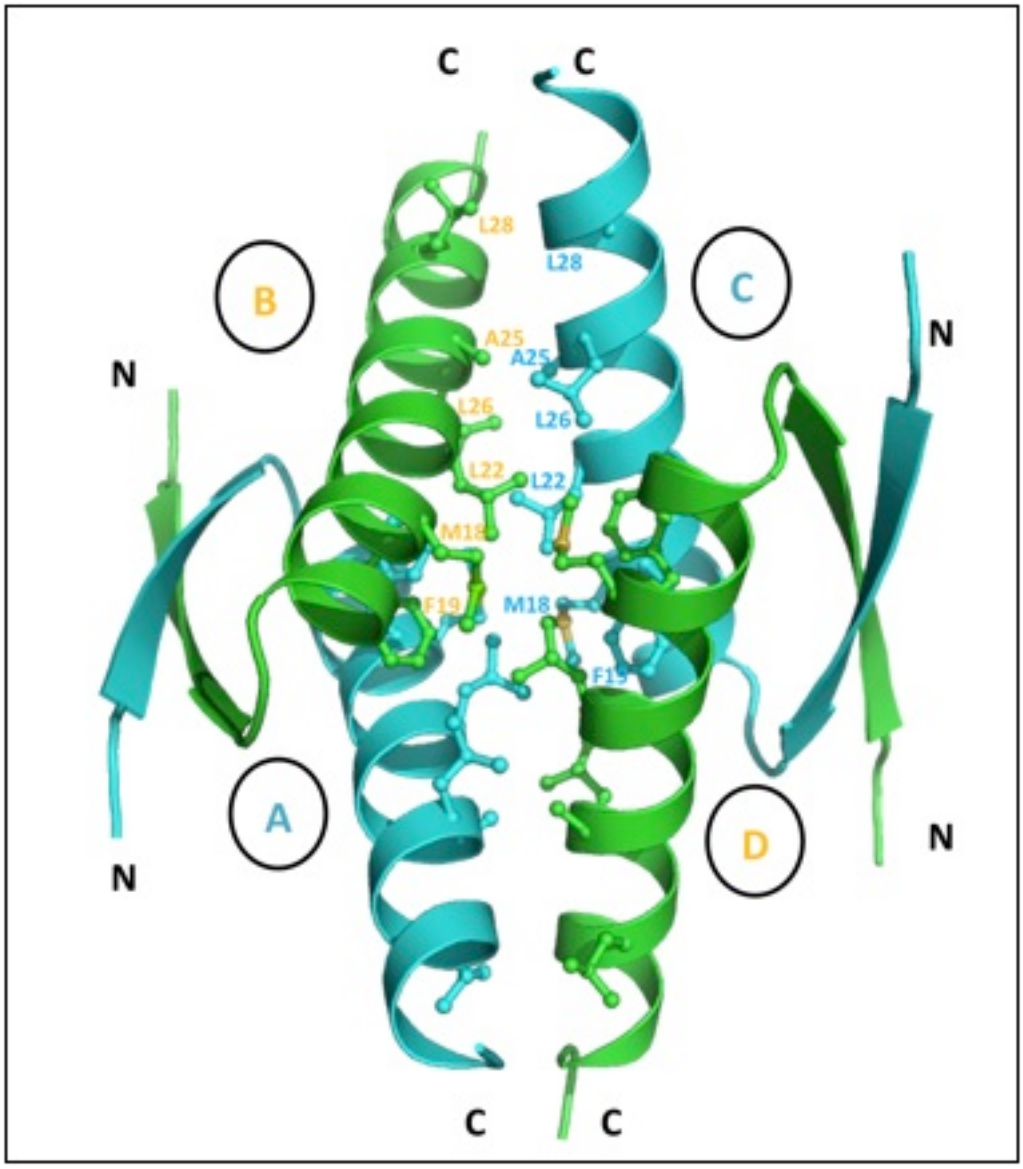


Figure 2.13. **Hydrophobic core of p53 tetramerization domain.** The residues forming the hydrophobic core of the tetramer are shown according to their chain color.

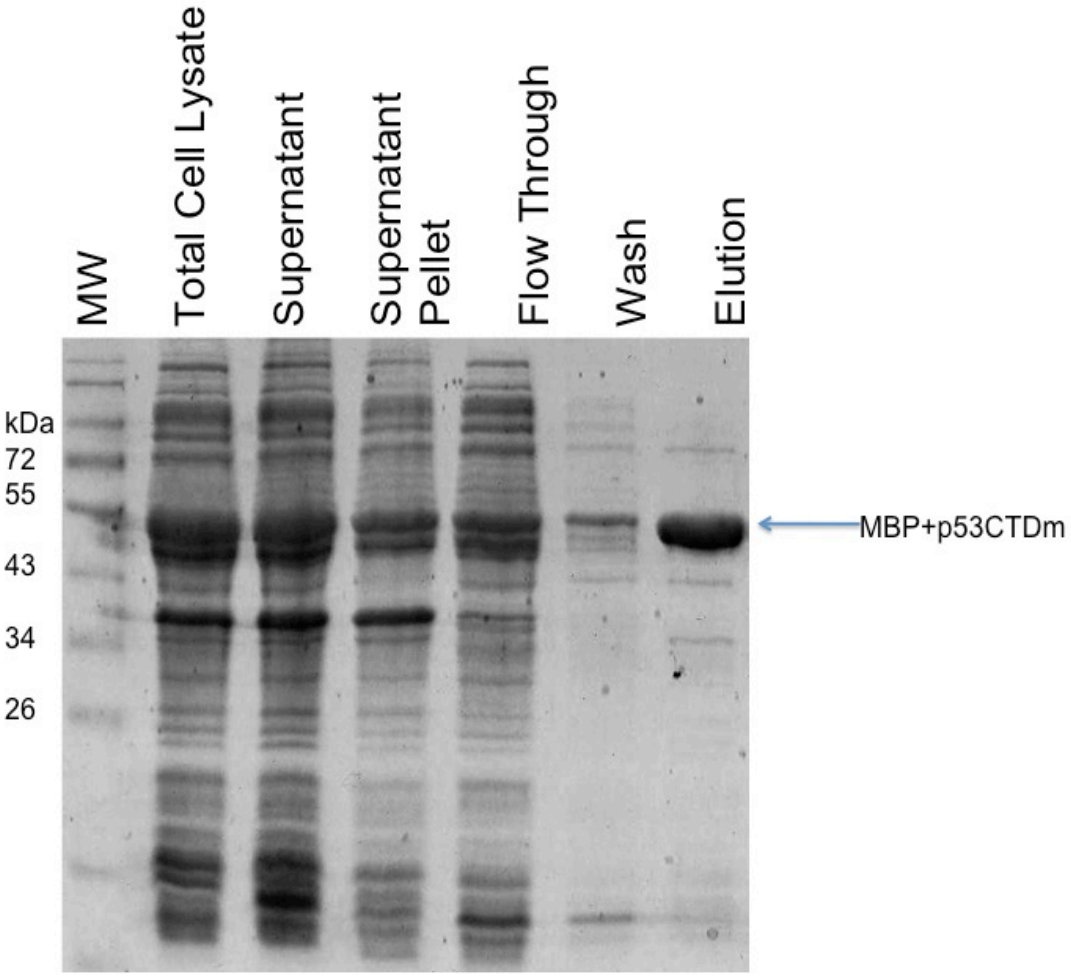


Figure 2.14. **SDS-PAGE analysis of purification of MBP-pp-p53CTD G360S/G361A mutant.** Protein was eluted with a solution of 50mM maltose and appeared at around 50 kDa upon SDS-PAGE analysis. Eluted protein was digested overnight with PreScission Protease.

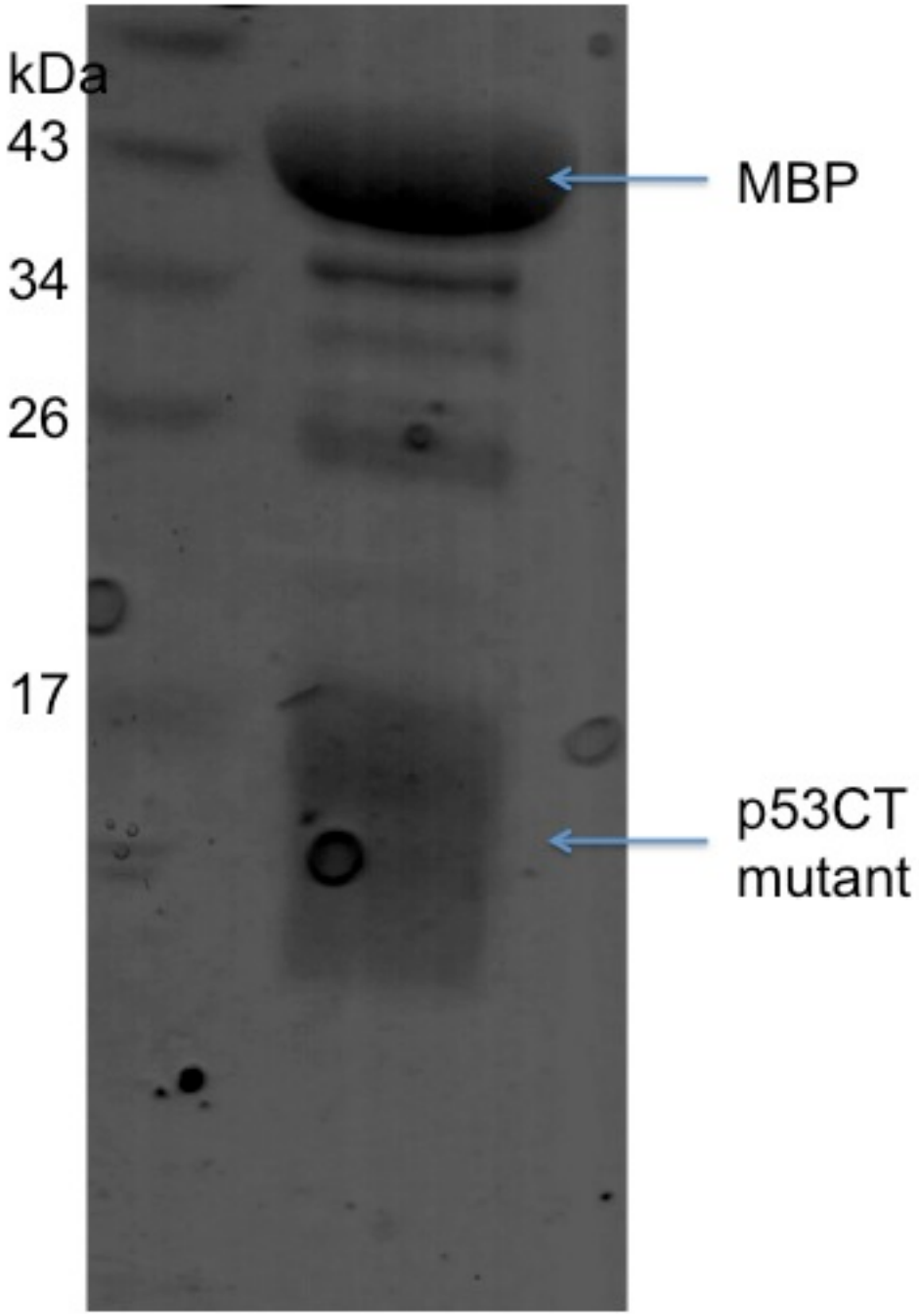


Figure 2.15. **SDS-PAGE analysis of digested MBP-pp-p53CTD mutant**. The protein was digested overnight with PreScission protease. p53CTD appeared at around 8kDa on the gel, and maltose binding protein appeared at around 43kDa. Several impurities bands were observed in gel as well.

Table 2.2. **Summary of DNA sequences used in the study of the interaction of p53CTD with DNA**

	Sequences	**MW (Da)**
Specific 14 bp DNA	AT**GGACATGTCC**AT	4262.8
Non-specific 14 bp DNA	TGCCCGTACGGGCA	4802.3
Specific 24 bp DNA	TC**GGGCATCCCCGGGCATGCCC**GA	7893.2

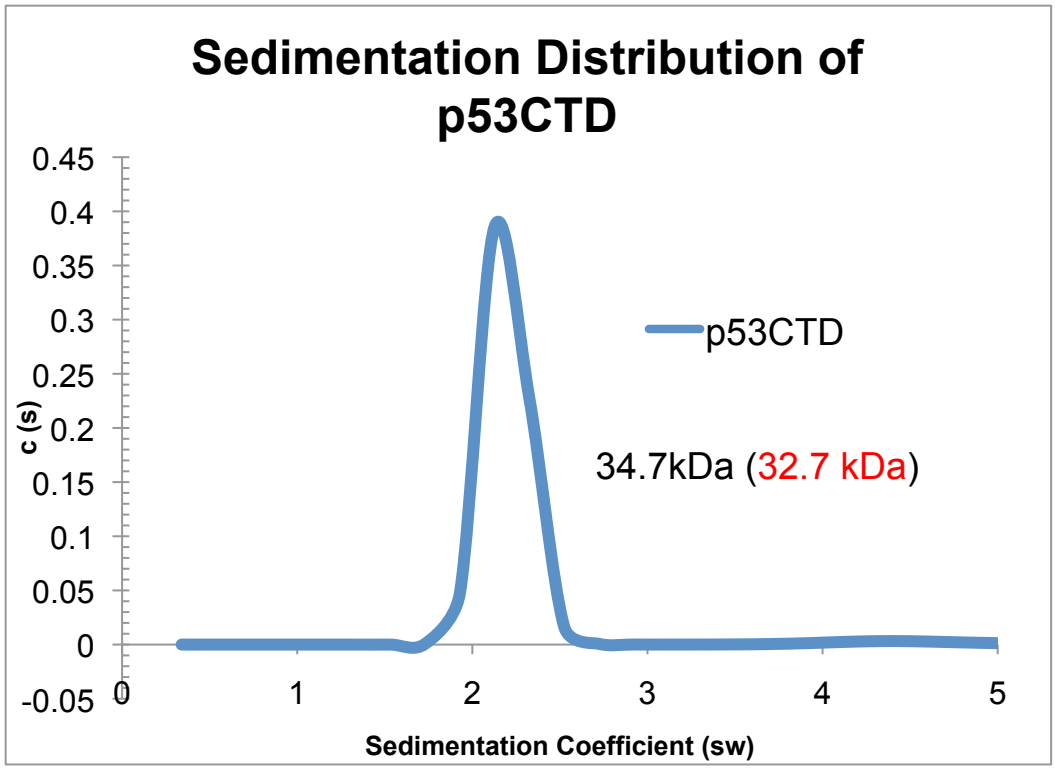


Figure 2.16. **Sedimentation Distribution of p53CTD obtained by SEDFIT program.** The p53 sedimentation velocity experiment was measured at 280nm. A peak at 2.25 sw indicates the presence of p53 tetramer with an experimental molecular weight of 34.7 kDa (black) compared to the theoretical molecular weight of 32.7 kDa (red). The p53 tetramer accounts for 78.495 % of the sample.

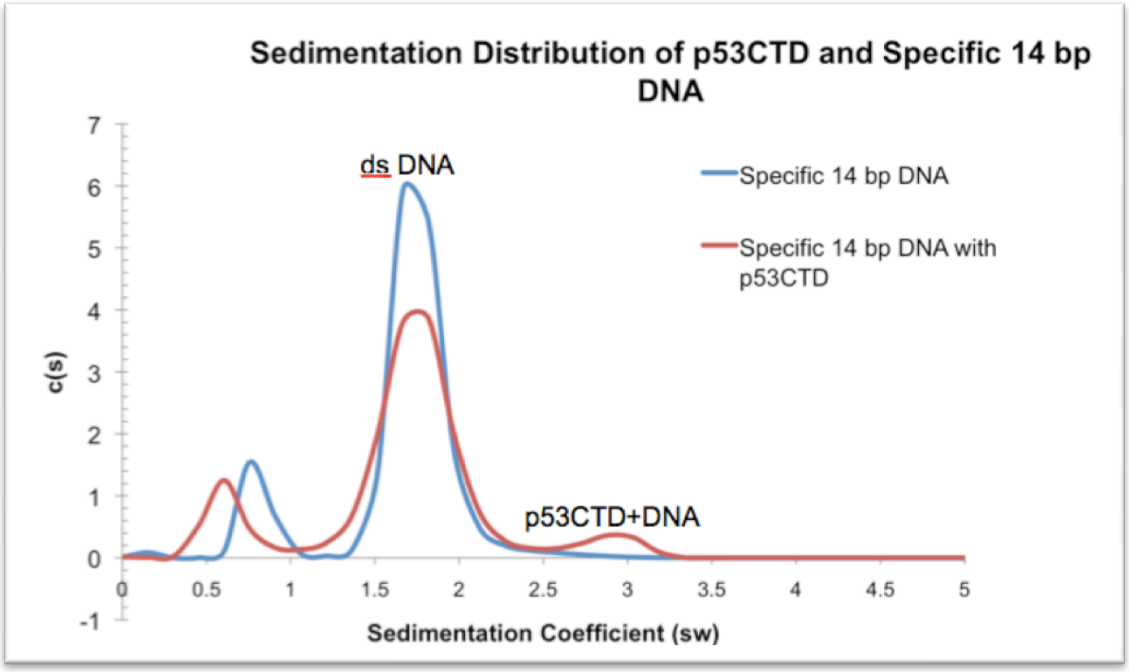


Figure 2.17. **Sedimentation Distribution of p53CTD and p53CTD complexed with specific 14 bp DNA obtained by SEDFIT program.** The experiment data was measured at 280nm. Three peaks were observed when the specific 14 bp DNA sequence was mixed with p53CTD (red), whereas two peaks were observed with the DNA alone (blue).

Table 2.3. **Summary of Sedimentation Distribution of p53CTD and p53CTD with specific 14 bp DNA.**

Protein/DNA	Theoretical Molecular Weight (kDa)	Experimental Sedimentation Coefficient (sw)	rmsd
specific 14 bp DNA	9.6	1.8	0.025733
p53CTD (dimer)/specific 14 bp DNA	25.2	2.7	0.018973

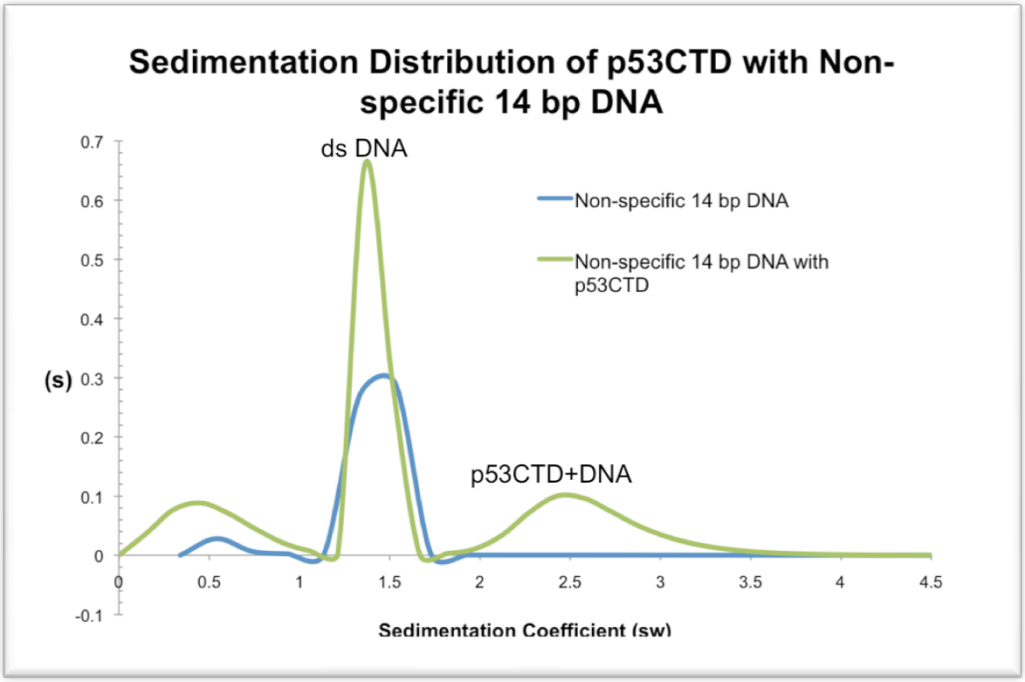


Figure 2.18. **Sedimentation distribution of p53CTD and p53CTD complexed with non-specific 14 bp DNA obtained by SEDFIT.** The experiment was run at 488 nm. Three peaks were observed when non-specific 14 bp DNA was mixed with p53CTD (green), whereas two peaks were observed for the DNA alone (blue).

Table 2.4. **Summary of sedimentation distribution of p53CTD and p53CTD with non-specific 14 bp DNA.** 28.447% of the protein sample found to be in the dimeric state in the presence of DNA.

Protein/DNA	Theoretical Molecular Weight (kDa)	Experimental Sedimentation Coefficient (sw)	rmsd
Non-specific 14bp DNA	9.6	1.6	0.00540
p53CT (dimer) with p53CTD-nonspecific14 bp DNA	25.2	2.5	0.006287

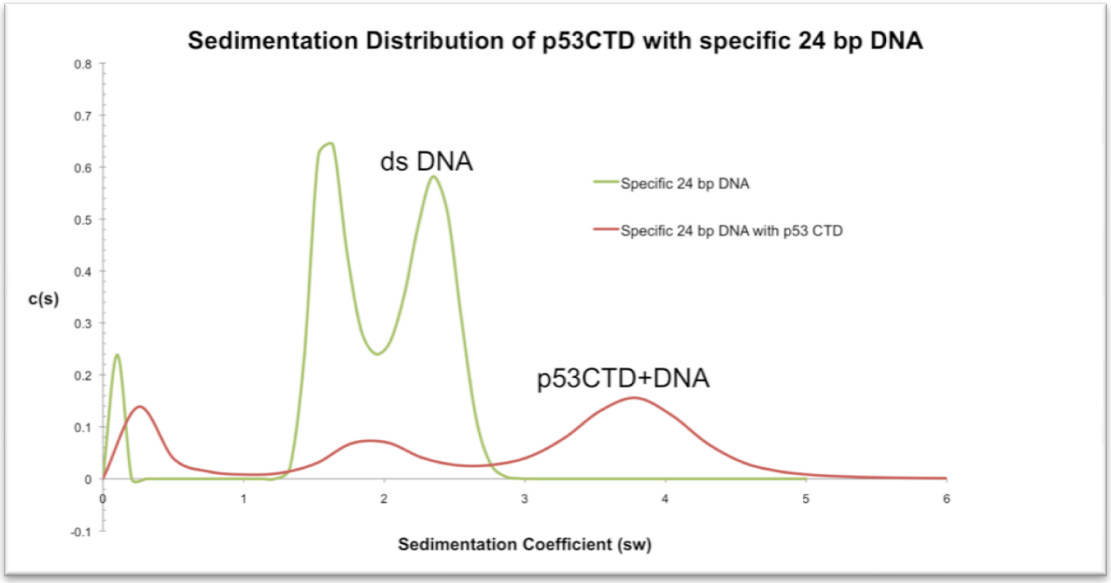


Figure 2.19. **Sedimentation Distribution of p53CTD and p53CTD complexed with specific 24 bp DNA obtained by SEDFIT program.** The experiment was run at 488 nm. Three peaks were observed when specific 24 bp DNA was mixed with p53 CTD (green), whereas two peaks were observed from DNA alone (red)

Table 2.5. **Summary of sedimentation distribution of p53CTD and p53CTD with specific 24 b.p. DNA**. 28.447% of sample was shown to be in the dimeric state in the presence of the DNA.

Protein/DNA	Theoretical Molecular Weight (kDa)	Experimental Sedimentation Coefficient (sw)	rmsd
Specific 24 bp DNA	15.8	2.2	0.005464
p53CTD with p53CTD-spec.24 bp DNA	32.1	3.9	0.005366

Discussion

We aimed to obtain structural information on the regulatory domain of p53. Although we crystallized p53CTD and obtained high resolution diffraction to 2.3Å, the structure of the p53CTD was not solved due to a problem of proteolysis during crystallization. A tetramer of p53CTD was observed in the crystal structure, but the regulatory domain electron density was absent. The orientation of the tetramerization domain in our crystal was the same as in the previous structure from Jeffrey et al. The hydrophobic nature of the dimer-dimer interaction in the tetramerization domain was also observed in the crystal structure. However, the structure of the regulatory domain was not determined in the crystal structure. This is possibly due to the unstructured and flexible regulatory domain of p53 (Bell et al., 2002). This region was in addition subject to proteolysis during crystallization, which is the major reason of the disappearance of the regulatory domain in the p53CTD crystal structure.

Our sedimentation distribution experimental data demonstrated that the p53CTD is in a dimeric state in the presence of DNA. These results were accurate because the root mean square deviation of the generated AUC data from SEDFIT had a rms deviation below 0.01 at a 95% confidence level. In addition, p53CTD exhibits an ability to bind non-specifically to DNA. It is also interesting to note that p53CTD did not undergo tetramerization in the presence of DNA, but rather stayed in its dimeric state. One intriguing possibility is that p53 may have different conformations in its active and inactive states. It would be interesting to study this hypothesis using fluorescence anisotropy. Such an

approach could potentially determine the binding affinity between different sequences or lengths of DNA with p53CTD and give insight into the properties of DNA sequences that might be used to induce more rigid secondary structural elements in p53CTD to aid in X-ray crystallography.

References

ADAMS, P. D., GROSSE-KUNSTLEVE, R. W., HUNG, L. W., IOERGER, T. R., MCCOY, A. J., MORIARTY, N. W., READ, R. J., SACCHETTINI, J. C., SAUTER, N. K. & TERWILLIGER, T. C. 2002. PHENIX: building new software for automated crystallographic structure determination. *Acta Crystallogr D Biol Crystallogr,* 58**,** 1948-54.

AHN, J. & PRIVES, C. 2001. The C-terminus of p53: the more you learn the less you know. *Nat Struct Biol,* 8**,** 730-2.

BELL, S., KLEIN, C., MULLER, L., HANSEN, S. & BUCHNER, J. 2002. p53 contains large unstructured regions in its native state. *J Mol Biol,* 322**,** 917-27.

CHEN, Y., DEY, R. & CHEN, L. 2010. Crystal structure of the p53 core domain bound to a full consensus site as a self-assembled tetramer. *Structure,* 18**,** 246-56.

CHO, Y., GORINA, S., JEFFREY, P. D. & PAVLETICH, N. P. 1994. Crystal structure of a p53 tumor suppressor-DNA complex: understanding tumorigenic mutations. *Science,* 265**,** 346-55.

CLORE, G. M., OMICHINSKI, J. G., SAKAGUCHI, K., ZAMBRANO, N., SAKAMOTO, H., APPELLA, E. & GRONENBORN, A. M. 1994. High-resolution structure of the oligomerization domain of p53 by multidimensional NMR. *Science,* 265**,** 386-91.

EMSLEY, P., LOHKAMP, B., SCOTT, W. G. & COWTAN, K. 2010. Features and development of Coot. *Acta Crystallogr D Biol Crystallogr,* 66**,** 486-501.

HUPP, T. R., LANE, D. P. & BALL, K. L. 2000. Strategies for manipulating the p53 pathway in the treatment of human cancer. *Biochem J,* 352 Pt 1**,** 1-17.

JEFFREY, P. D., GORINA, S. & PAVLETICH, N. P. 1995. Crystal structure of the tetramerization domain of the p53 tumor suppressor at 1.7 angstroms. *Science,* 267**,** 1498-502.

LAUE, T. M., SHAH, B. D., RIDGEWAY, T. M. & PELLETIER, S. L. 1992. Computer-Aided Interpreation of Analytical Sedimentation Data for Proteins in Analytical Ultracentrifugation. *Royal Society of Chemistry*

LEBOWITZ, J., LEWIS, M. S. & SCHUCK, P. 2002. Modern analytical ultracentrifugation in protein science: a tutorial review. *Protein Sci,* 11**,** 2067-79.

MATTHEWS, B. W. 1968. Solvent content of protein crystals. *J Mol Biol,* 33**,** 491-7.

MAY, P. & MAY, E. 1999. Twenty years of p53 research: structural and functional aspects of the p53 protein. *Oncogene,* 18**,** 7621-36.

MCCOY, M., STAVRIDI, E. S., WATERMAN, J. L., WIECZOREK, A. M., OPELLA, S. J. & HALAZONETIS, T. D. 1997. Hydrophobic side-chain size is a determinant of the three-dimensional structure of the p53 oligomerization domain. *EMBO J,* 16**,** 6230-6.

MCKINNEY, K., MATTIA, M., GOTTIFREDI, V. & PRIVES, C. 2004. p53 linear diffusion along DNA requires its C terminus. *Mol Cell,* 16**,** 413-24.

MURSHUDOV, G. N., VAGIN, A. A. & DODSON, E. J. 1997. Refinement of macromolecular structures by the maximum-likelihood method. *Acta Crystallogr D Biol Crystallogr,* 53**,** 240-55.

OTWINOWSKI, Z. & MINOR, W. 1997. Processing of X-ray Diffraction Data Collected in Oscilliation Mode. *Methods Enzymol,* 276**,** 307-326.

SAKAMOTO, H., LEWIS, M. S., KODAMA, H., APPELLA, E. & SAKAGUCHI, K. 1994. Specific sequences from the carboxyl terminus of human p53 gene product form anti-parallel tetramers in solution. *Proc Natl Acad Sci U S A,* 91**,** 8974-8.

TERWILLIGER, T. C. 2000. Maximum-likelihood density modification. *Acta Crystallogr D Biol Crystallogr,* 56**,** 965-72.

TERWILLIGER, T. C. 2003. Automated main-chain model building by template matching and iterative fragment extension. *Acta Crystallogr D Biol Crystallogr,* 59**,** 38-44.

TERWILLIGER, T. C. & BERENDZEN, J. 1999. Automated MAD and MIR structure solution. *Acta Crystallogr D Biol Crystallogr,* 55**,** 849-61.

VAN DUYNE, G. D., STANDAERT, R. F., KARPLUS, P. A., SCHREIBER, S. L. & CLARDY, J. 1993. Atomic structures of the human immunophilin FKBP-12 complexes with FK506 and rapamycin. *J Mol Biol,* 229**,** 105-24.

VOGELSTEIN, B., LANE, D. & LEVINE, A. J. 2000. Surfing the p53 network. *Nature,* 408**,** 307-10.

WANG, P., REED, M., WANG, Y., MAYR, G., STENGER, J. E., ANDERSON, M. E., SCHWEDES, J. F. & TEGTMEYER, P. 1994. p53 domains: structure, oligomerization, and transformation. *Mol Cell Biol,* 14**,** 5182-91.

Chapter Three
Expression and Purification of p53 Variants

Introduction

The regulatory domain of p53 influences the efficiency of p53 to act as a sequence-specific DNA binding transcription factor. Its post-translational modifications and interactions with other proteins are the critical factors in promoting the stability of p53-DNA complexes (Vogelstein et al., 2000, Ko and Prives, 1996). Fundamental questions regarding the role of p53 regulatory domain remain to be answered. The determination of the structure of the regulatory domain would create a framework to pose more specific questions on the regulatory mechanism in p53. As described in Chapter 2, we attempted to determine the structure of the tetramerization domain and the regulatory domain of p53 (p53CTD). Besides exploring the biophysical characteristics of p53CTD, we also generated other p53 variants that would allow us to explore the nature of the regulatory domain associating with the DNA binding domain in p53. Three variants generated are: full length of p53 with 8x His tagged, MBP-pp-p53 94-393, and MBP-pp-p53 94-393Δ28 (Figure 3.1). Through these constructs, we are interested in understanding how the C-terminal domain of p53 regulates the DNA binding of the core domain. The final goal of the variants described in this chapter is to pursue our goal in determining the atomic structure of the full length p53 and all its domains.

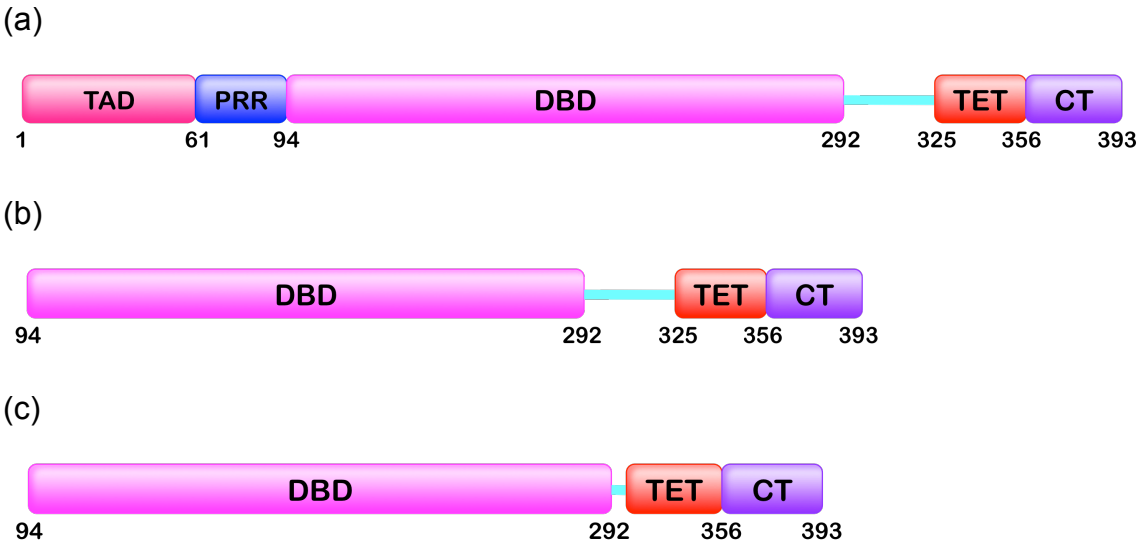


Figure 3.1. **Domain Organization of p53 variants**. (a) Full length of p53. (b) p53 94-393. (c) p53 94-393Δ28.

Materials and Methods

Full length of p53 with 8xHis-tag

Cloning

The DNA sequence encoding amino acids 1 to 393 of full length human p53 was amplified via PCR. The amplified DNA fragment was cloned into the pET-28 expression vector (Novagen) using *Eco*RI and *Hind*III as cloning sites. The plasmid with the cloned gene was sequenced and then transformed into the BL21(DE3) *E. coli* strain (Stratagene).

Expression and Purification

We used the same expression protocol that was previously described for p53CTD.

E. coli cells were lysed using a French press after the addition of 0.4 mM PMSF. Cell lysate was clarified by ultracentrifugation at 30000 r.p.m. for 30 minutes at 4°C. The first step of purification was carried out by affinity purification incubation with agitating the cell supernatant with 1mL of Ni-NTA resin (QIAGEN) at 4 °C for 1 hour. The resin bound to the protein was transferred to a gravity column where the supernatant was drained and the resin washed with 100 mL of high salt buffer and then with 50mL of in the same high salt buffer containing 40mM imidazole. Protein was eluted using 15mL high salt buffer in 3mL fractions with increasing imidazole concentrations (100 mM – 500 mM). Fractions containing the targeted 8xHis tagged full length p53 were negatively stained and examined under the electron microscope.

MBP-p53 94-393 and MBP-p53 94-393Δ28 variants

Cloning

MBP-p53 94-393 was subcloned from the original plasmid while MBP-p53 94-393Δ28 plasmid was generated by Quikchange Site-Directed Mutagenesis (Stratagene).

Expression and purification

Expression and purification of p53 variants followed the protocol of p53CTD as described in Chapter 2.

Results

Full length of p53 with 8xHis-tag

With a protocol modified from the one established by the postdoctoral fellow Armando Lucumi in our laboratory, the full length of p53 tagged with 8xHis was successfully purified using Ni-NTA agarose using 500mM NaCl, 50mM Tris HCl, 20mM imidazole, and pH 8.0 buffer (Figure 3.2). Most proteins were eluted with the buffer containing 100mM imidazole. However, some degradation was detected in the western blot (Figure 3.3). Proteins eluted from 400mM imidazole elution buffer were negatively stained for electron microscopy (data not shown).

MBP-pp-p53 94-393 precipitated after overnight digestion

MBP-pp-p53 94-393 contains three major domains: DNA binding domain, tetramerization domain and the regulatory domain. Proteins were successfully

purified following same method as p53CTD (Figure 3.4). However, MBP-pp-p53-94-393 precipitated after overnight digestion by Prescission protease, and it was not possible to purify.

MBP-p53 94-393 ∆28 precipitated after overnight digestion

MBP-p53 94-393 ∆28 contains the same domain organization as MBP-pp-p53 94-393. However, residues 292-325 were deleted in this construct. By reducing the linker size, we aimed to reduce the flexibility of the protein and increase its likelihood to crystallize. MBP-p53 94-393∆28 was successfully purified following the same method as p53CTD. However, MBP-p53 94-393∆28 was completely precipitated after overnight digestion by Prescission protease. MBP-p53 94-393∆28 was found in the precipitant and it was not possible to continue with its purification (Figure 3.5).

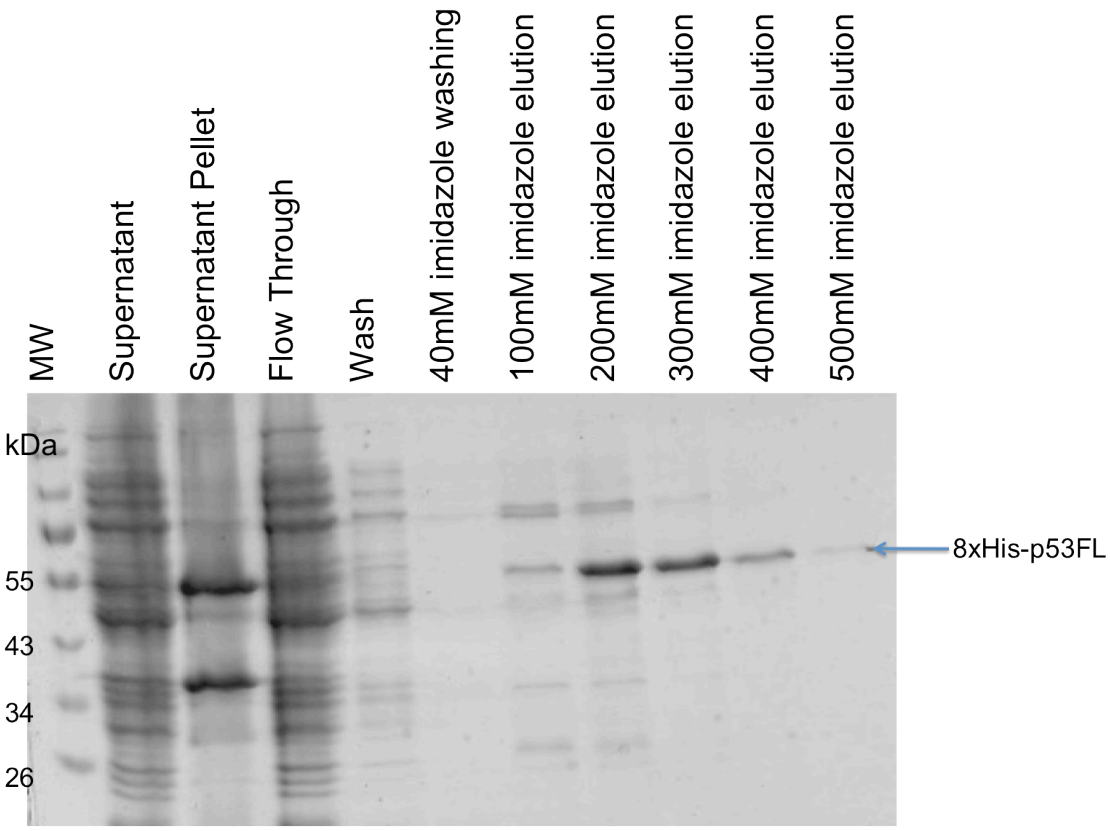


Figure 3.2. **SDS-PAGE analysis of 8xHis-tagged full length p53 purification.** Protein was stepwise eluted from Ni-NTA resin using an increasing imidazole concentration of 100 to 500mM. 8xHis tagged full length p53 appeared at around 55kDa on the gel.

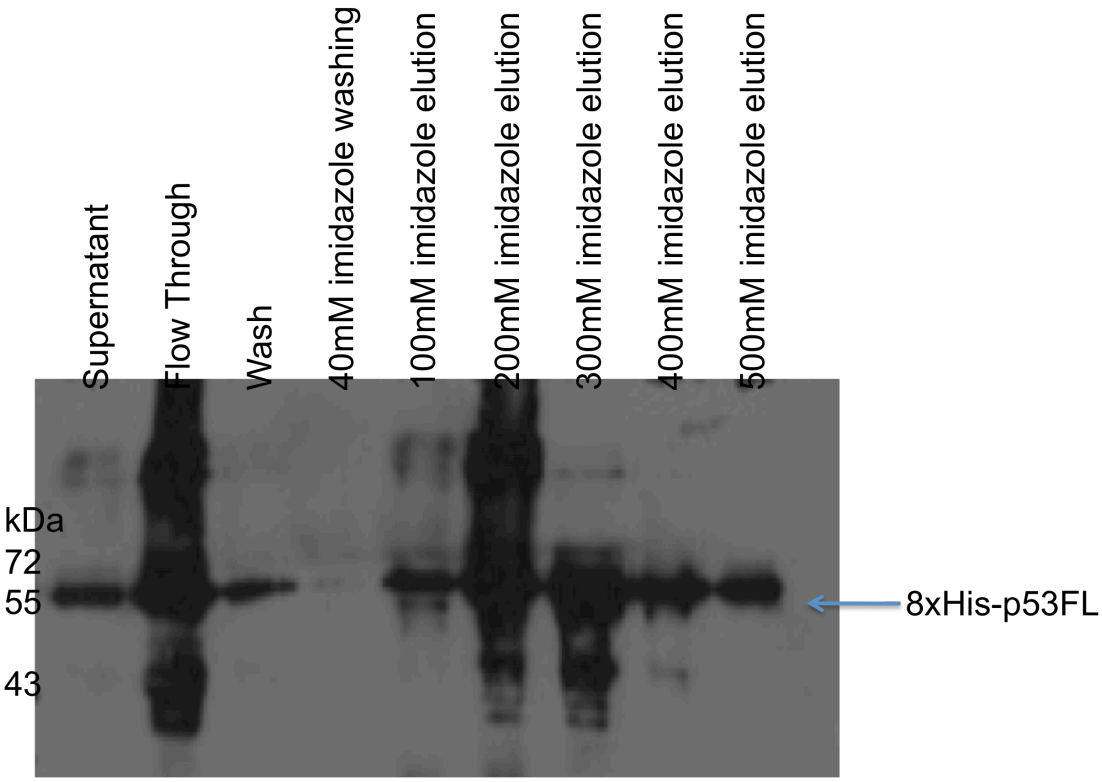


Figure 3.3. **Western analysis of 8xHis tagged full length p53 purification.** Western blot detection of 8xHis tagged full length p53 purification using Anti-His antibody.

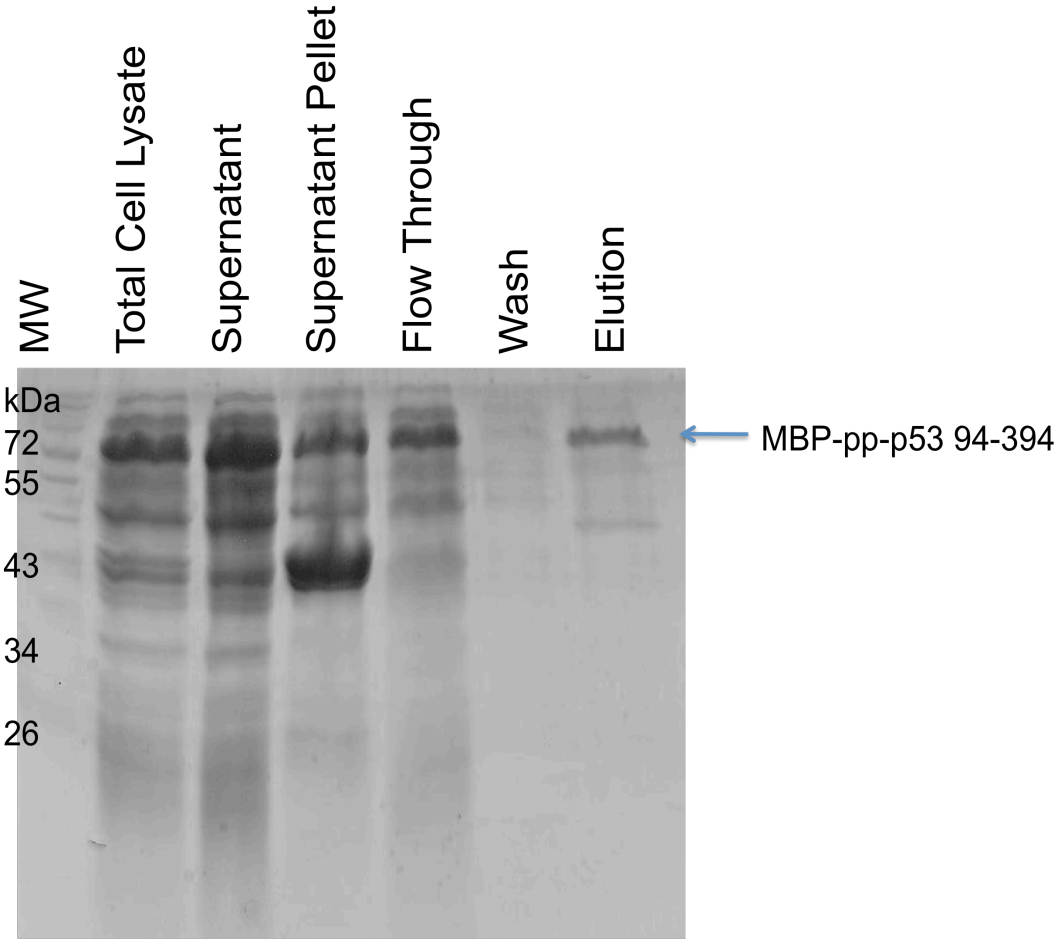


Figure 3.4. **SDS-PAGE analysis of MBP-pp-p53 94-393 purification.** Protein was eluted from amylose resin using 50mM maltose elution buffer. p53-94-393 tagged with MBP appeared at 72kDa on gel.

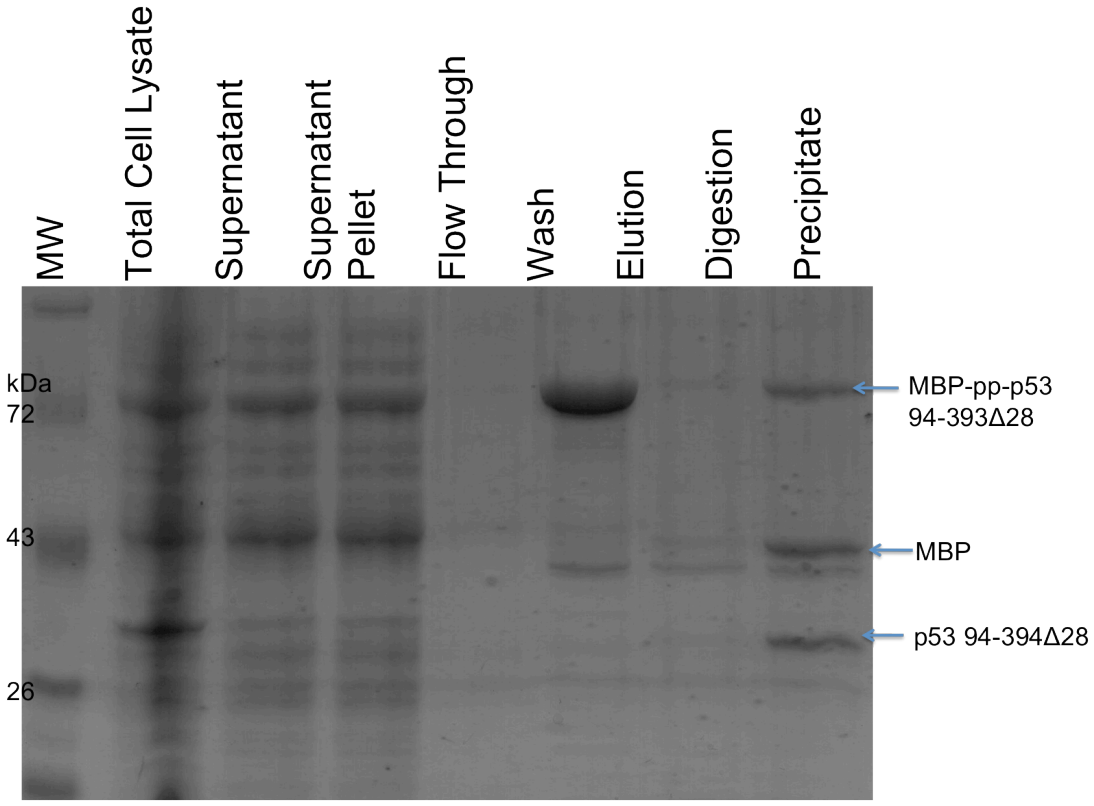


Figure 3.5. **SDS-PAGE analysis of MBP-pp-p53 94-393Δ28 purification.** Protein was eluted from amylose resin using 50mM maltose elution buffer. p53-94-393Δ28 with MBP tagged appeared at 72kDa on gel. After digestion, p53-94-393Δ28 precipitated.

Discussion

After many experimental trials, 8xHis tagged p53 full length was successfully purified. Although we did not get enough yield of protein for crystallization, it was sufficient enough for electron microscopy. Currently, a graduate student in our laboratory is pursuing the three-dimensional reconstruction of full-length p53.

Several deletion variants of p53 were designed for our structural studies. As reported, our initial attempts at purifying these variants were not successful. More experiments have to be done in the future to establish the purification system of these variants. Interestingly, two constructs of p53 containing residues 94 to 393 and residues 94 to 393 with deletion of 28 residues have the same purification behavior. Both proteins precipitated after overnight digestion from the MBP tag. To avoid precipitation, detergent-like chemicals such as CHAPS and Triton were added to the MBP-pp-94-393 digestion, but they did not help in maintaining the protein in solution. Same precipitation occurred upon the addition of DNA before the digestion. These results suggest that constructs containing residues 94-393 are unfolded. Therefore, we need to continue exploring conditions that will allow successful purification of these constructs. More experiments have to be conducted to further understand the biophysical characteristics of these two constructs.

References

KO, L. J. & PRIVES, C. 1996. p53: puzzle and paradigm. *Genes Dev,* 10**,** 1054-72.

VOGELSTEIN, B., LANE, D. & LEVINE, A. J. 2000. Surfing the p53 network. *Nature,* 408**,** 307-10.

Chapter Four

Understanding the Oligomerization state of MDM2 by Analytical Ultracentrifugation and Electron Microscopy

Introduction

4.1 Functions and Pathway of MDM2

MDM2 (Murine Minute Double 2) was the first identified as negative regulator of p53 with oncogenic properties (Momand et al., 1992). In the absence of cellular stresses, MDM2 regulates p53 by binding to the p53 transactivation domain and acting as an E3 ubiquitin ligase that triggers proteasomal degradation (Cheng et al., 2009, Momand et al., 1992) (Figure 4.1).

Upon cellular stress, MDM2 is phosphorylated by several DNA-damage-induced kinases, such as: ataxia-telangiectasia mutated (ATM) kinase, ATM and Rad3-related kinase, the DNA-dependent kinase (DNA-PK) and c-Abl (Lehman et al., 2008). One particular p53 pathway that acts in response to DNA damage is activated by ATM kinase. ATM phosphorylates the MDM2 RING domain at residue S395 (Lehman et al., 2008). This phosphorylation is speculated to inhibit MDM2 oligomerization and prevent the scaffold formation for ubiquitination elongation, which increases the level of p53 in cell for cell degradation (Figure 4.2). Furthermore, MDM2 can self- or auto-ubiquitinates itself for proteasomal degradation in order to release p53 for further cellular regulation during cellular stresses (Clegg et al., 2008).

4.2 Structure of MDM2

Human MDM2 is a polypeptide of 491 amino acids with a molecular weight of 56 kDa. It consists of four domains: Transactivation domain (TAD, residues 1-100), Central Acidic Domain (CAD, residues 230-300), Zinc Finger

Domain (residue 290-335), and RING domain (residues 430-480). It also includes a nuclear localization sequence and a nuclear export sequence between TAD and CAD.

Transactivation domain

MDM2 N-terminal Transactivation domain (TAD, residues 1-109) is responsible for p53 binding through p53 TAD. This MDM2:p53 interaction regulates p53 ubiquitin-dependent degradation. (Lane et al., 2010) (Figure 4.3). Several structures of MDM2 TAD in complex with a short p53 N-terminus peptide or an inhibitor such as nutlin have been solved at high resolution using X-ray crystallography (Kussie et al., 1996, Shangary et al., 2008, Vassilev et al., 2004). These structures have clearly shown that the MDM2 TAD embodies a hydrophobic cleft, where a triad of hydrophobic and aromatic residues of p53 (Phe19, Trp23, and Leu26) insert deep into MDM2 (Kussie et al., 1996).

Central Acidic Domain (CAD)

The MDM2 central acidic domain is the key domain responsible for MDM2 function. It contains several phosphorylation sites (Lane et al., 2010). In addition, the CAD is necessary for the interactions of MDM2 with other signaling proteins such as ribosomal protein L5, p300/CBP and p19ARF in response to ribosomal stress (Iwakuma and Lozano, 2003, Kulikov et al., 2006, Nicholson and Hupp, 2010).

Zinc Finger Domain

The major function of MDM2 Zinc Finger domain (residue 290-335) is still unclear. However, this region contains a conserved residue C305 from different species which coordinates with zinc (Lane et al., 2010). Recently, the structure of the Zinc Finger Domain was determined by NMR (Yu et al., 2006). The structure reveals a zinc ribbon structural motif which is one of the largest groups of zinc fingers (Krishna et al., 2003). The Zinc Finger domain is believed to play a significant role in interacting with ribosomal proteins and mediating a wide variety of protein-protein, protein-DNA, and protein-RNA interactions (Yu et al., 2006).

RING domain

The RING domain (residues 429-491) is located at the C-terminus of MDM2 which facilitates the oligomerization of MDM2 and thus controls the activity of its polyubiquintation and regulation of p53 proteasomal degradation (Cheng et al., 2009). The RING domain can also bind to nucleotides such as ATP, which is important for MDM2 nuclear localization (Poyurovsky et al., 2007). Furthermore, the RING domain can mediate the complex formation between MDM2 and MDMX (Sharp et al., 1999, Jackson and Berberich, 2000, Stad et al., 2000, Tanimura et al., 1999).

Efforts towards structural studies of MDM2

Recently, several crystal structures of MDM2 TAD with a short p53 N-terminal peptide (residues 1-32) and the RING domain have determined through

X-ray crystallography. However, the structure of full-length of MDM2 is still to be determined. Although we understand how MDM2 binds to the p53 transactivation domain, we have limited knowledge on how MDM2 facilitates the polyubiquination of p53 and how the tetrameric p53 binds to MDM2. Structural studies of full-length MDM2 are crucial to further understand its dynamic molecular functions in cells, which would aid anticancer drug development.

Recently, one research group has carried out several biochemical studies of MDM2 RING domain. Surprisingly, recombinant MDM2 RING domain assembles into large molecular weight complex, as observed by both gel filtration chromatography and electron microscopy (Poyurovsky et al., 2007). This interesting phenomenon stimulated our interest in studying the oligomerization state of full-length MDM2 by single particle electron microscopy and analytical ultracentrifugation. In order to carry out these experiments, we first established an MDM2 expression and purification system in *E. coli*.

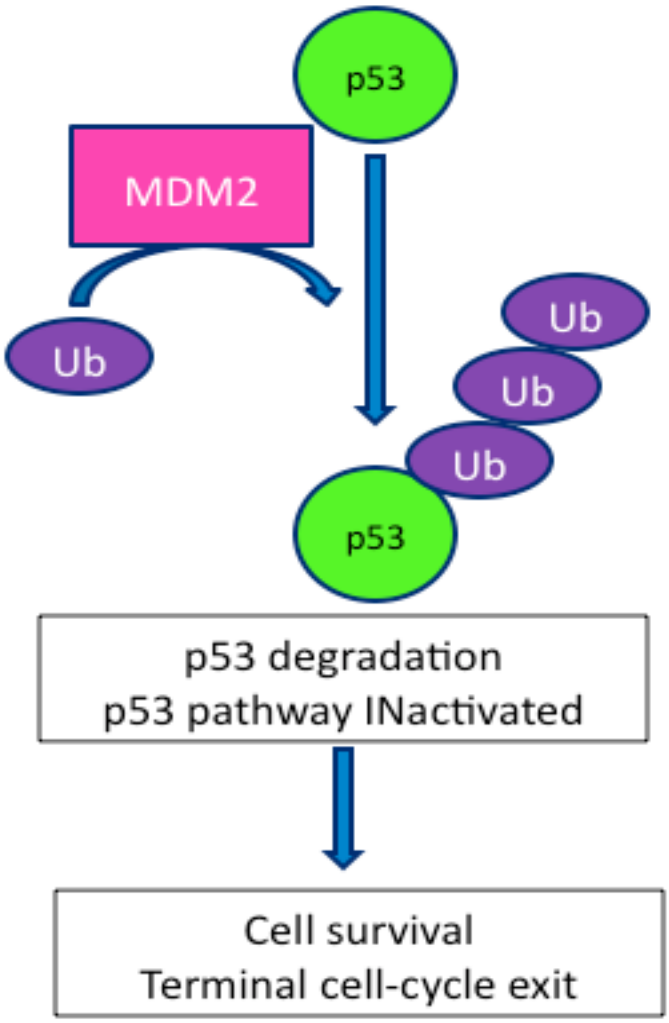


Figure 4.1. **MDM2 in resting cells**. Upon cellular stresses, MDM2 promotes polyubiquitination of the regulatory domain of p53 to facilitate p53 proteasomal degradation and consequently, cell survival.

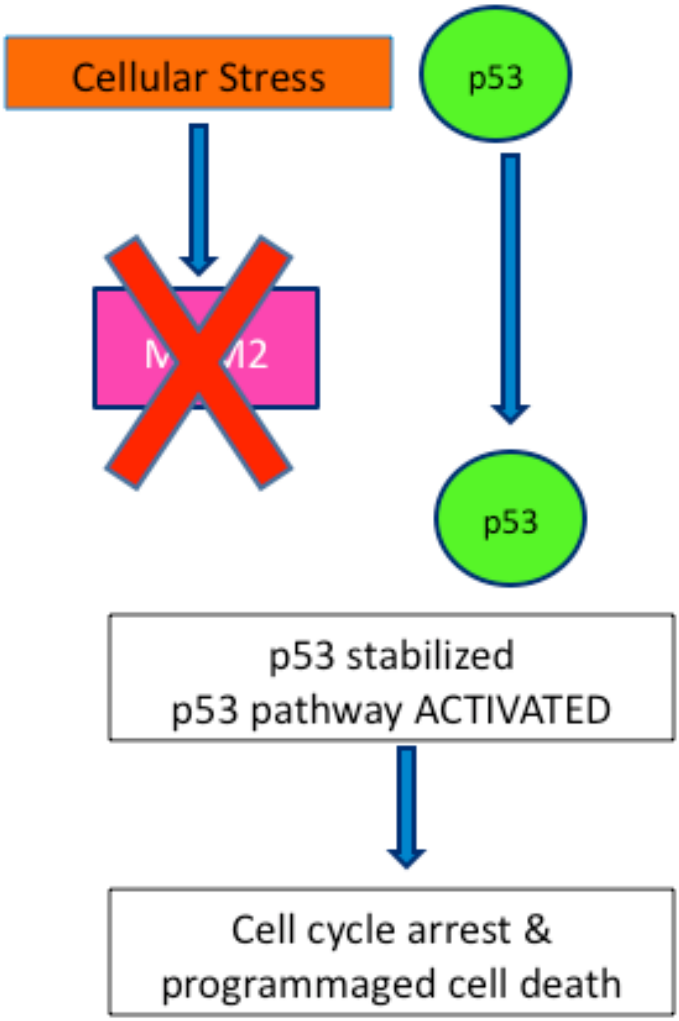


Figure 4.2. **MDM2 after DNA damage**. MDM2 is phosphorylated which disrupts MDM2 oligomerization. Inhibition of p53 is thus suppressed, resulting in p53-mediated cell death.

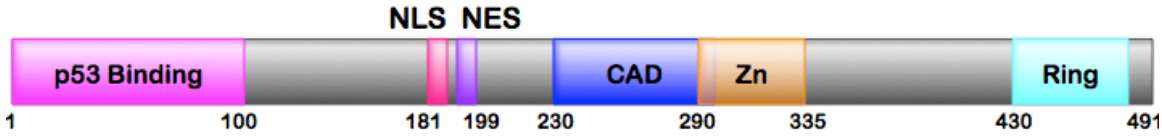


Figure 4.3. **Domain Organization of Human MDM2**. MDM2 is a polypeptide chain of 491 amino acids, consisting of four domains: Transactivation domain/p53 binding domain, acidic domain, Zinc finger domain, and RING domain.

Materials and Methods

Cloning

A DNA sequence encoding the human MDM2 was cloned into the pET28 bacterial expression vector using EcoRI and HindIII cloning sites.

Expression and Purification of Human MDM2

The MDM2 plasmid was transformed into *Escherichia coli* BL21(DE3) cells. Cells were initially grown in YT medium at 37°C. And cells were induced with 0.5mM isopropyl-1-thio-β-D-galactopyranoside (IPTG) when O.D. was 0.6, and grown for 4 hours at 25 °C. The cells were collected by centrifugation and resuspended in high salt buffer (500 mM NaCl, 50 mM Tris-HCl (pH 8.0), 20 mM Imidazole). Cells were lysed with a French press with the addition of 0.04 mM phenyl-methanesulfonylfluoride (PMSF). Cell lysate was clarified by ultracentrifugation at 30000 r.p.m. for 30 minutes at 4°C. The cell supernatant was batch bound with 1mL of Ni-NTA resin (QIAGEN) and incubated at 4 °C for 1 hour and transferred to a gravity column. The supernatant was drained and the resin was first washed with 100mL of high salt buffer and then 50 mL of 40 mM imidazole in addition to the high salt buffer. Protein was eluted using 15 mL high salt buffer with increasing imidazole concentration (100 mM – 500 mM) and 3mL fractions were collected. Fraction containing targeted 8His-MDM2 were pull together and concentrated to 1mL using Amicon Ultra (10k) and loaded onto a Superose 6 column for further purification. Fractions collected from the column were analyzed by SDS-PAGE followed by Coomassie staining.

Size Exclusion Chromatography

Analytical measurements were performed by using FPLC chromatography and Superose 6 column. Samples were directly injected onto the column and separated at room temperature at a flow rate of 0.5 mL/min while absorbance was recorded at 280nm.

Electron Microscopy

Formvar-coated copper grids were glow discharged, floated on sample drops for minutes, blotted, and air-dried in advance. Samples were then negatively stained for 20 seconds with 1% (w/v) aqueous uranyl acetate. Grids were photographed using a FEI Sphera electron microscope at 200kV.

Mass Spectrometry

From the same 10% SDS-PAGE that containing post-column samples were cut to 1mm x 1mm cubes and destained by washing with 100 µL of 100 mM ammonium bicarbonate for 15 minutes, followed by a second wash with the same volume of acetonitrile (ACN) for another 15 minutes. This process was repeated 3 times. The supernatant was discarded and the samples were dried in a speedvac for 15 minutes. Samples were then reduced by mixing with 200 µL of 100 mM ammonium bicarbonate/10 mM DTT and incubating in a 56 °C water bath for additional 30 minutes, followed by removal of supernatant. 200 µL of 100 mM ammonium bicarbonate/55 mM idocaetamide were added to gel pieces and incubated at room temperature covered with aluminum foil for 20 minutes. The

supernatant was removed, and the gel pieces were washed with 100 mM ammonium bicarbonate for 15 minutes followed by the same volume of ACN to dehydrate the gel pieces. The solution was then removed and samples were dried in speedvac for 15 minutes. For trypsin digestion, ice-cold trypsin (0.01µg/µL) in 50mM ammonium bicarbonate was added to cover the gel pieces and incubate on ice for 30 minutes. After compete rehydration, the excess trypsin solution was removed, replaced with fresh 50mM ammonium bicarbonate, and incubated overnight in 37°C. The resulting MDM2 peptides were extracted twice by the addition of 50 µL of 0.2% formic acid and 5% ACN followed by vortexing at room temperature for 30 minutes. The supernatant was removed and saved in a new eppendorf tube. A total of 50 µL ACN/0.2% formic acid was added to the sample and vortexed again at room temperature for 30 minutes. The combined extractions were analyzed directly by liquid chromatography (LC) in combination with tandem mass spectrometry (MS/MS) for electrospray ionization.

Analytical Ultracentrifugation (AUC)

Samples were prepared as described above. Proteins were concentrated around 0.10 Abs_{280} and analyzed by sedimentation velocity. Experiments were carried out under 20°C in a Beckman Optima-XL-I analytical ultracentrifuge. Sample (400 µL) and buffer (400 µL) were loaded into a double-sector centerpiece. The cells were loaded into an AN50Ti analytical rotor and accelerated to 50,000 rpm. Scans were acquired in continuous mode at 280nm for appropriate signals in the range of 0.1 to 1 absorption. The collected data were analyzed using the Lamm

Equation by using c(s) program at SEDFIT to determine the sedimentation coefficients. The partial specific volume, buffer viscosity, and buffer density were calculated through SEDNTERP.

Results

MDM2 was successfully purified using a high salt buffer

8His tagged full length MDM2 was expressed in *E. coli*. As previous experiments demonstrated that MDM2 degrades easily in buffer of 150mM NaCl, 50mM Tris-HCl (pH 8.0) (data not shown). To prevent protein degradation, buffer containing higher salt content,500 mM NaCl supplemented with 20 mM imidazole was used as lysis buffer. Purer MDM2 with 8His tag was eluted with 100 mM to 200 mM imidazole elution buffer from nickel resin (Figure 4.4). Proteins were concentrated to 1 mL to load onto the pre-equilibrated Superose 6 column to separate the impurities and aggregated proteins. Comparing the elution profiles between the purified MDM2 with the oligomerized standard allowed us to determine the molecular weight of the samples. MDM2 eluted as a broad peak centered at 23 mL, which upon comparison with the protein standards, indicates that the oligomeric MDM2 has an approximate molecular weight of 690 kDa. This result has confirmed that MDM2 eluted as an oligomers. Samples from the MDM2 broad peak were analyzed by SDS-PAGE analysis, which is clearly shown that the purified protein is from fraction 24 to 32 (Figure 4.6).

MDM2 has a molecular weight of 56 kDa but appears as 95 kDa in SDS-PAGE

MDM2 is calculated to be a 56 kDa protein. However, it appears as two double bands at 90 kDa in 10% SDS-PAGE. It is suggested that the disulfide bonds in the cysteine residues were not completely reduced by β-ME and SDS in the loading dye. To further confirm the presence of 8His-MDM2, samples were analyzed by electrospray ionization using tandem mass spectrometry. Most of the digested peptides were confirmed as human MDM2 E3 ubiquitin ligase. (Figure 4.5).

MDM2 appears as an oligomer under Analytical Ultracentrifugation

Post-column samples from fraction 20 to 32 were pooled together and concentrated to approximately 0.2 Abs_{280} for sedimentation velocity experiments. 80 scans of each sample were used to analyze using c(s) model. The partial specific volume, buffer density, and buffer viscosity were corrected to standard conditions (water at 20°C). Four peaks were observed. Based on the molecular weight of monomer of MDM2, the first peak is likely to be dimer, followed by trimer, tetramer and larger oligomers (Figure 4.7).

MDM2 displays spherical bodies with different sizes under Electron Microscopy

Sample from the same batch was also negatively stained for Electron Microscopy. Under EM, spherical bodies with different sizes were observed

(Figure 4.8). This result agrees with the gel filtration profile of MDM2, suggesting that the protein is forms an oligomer *in vitro*.

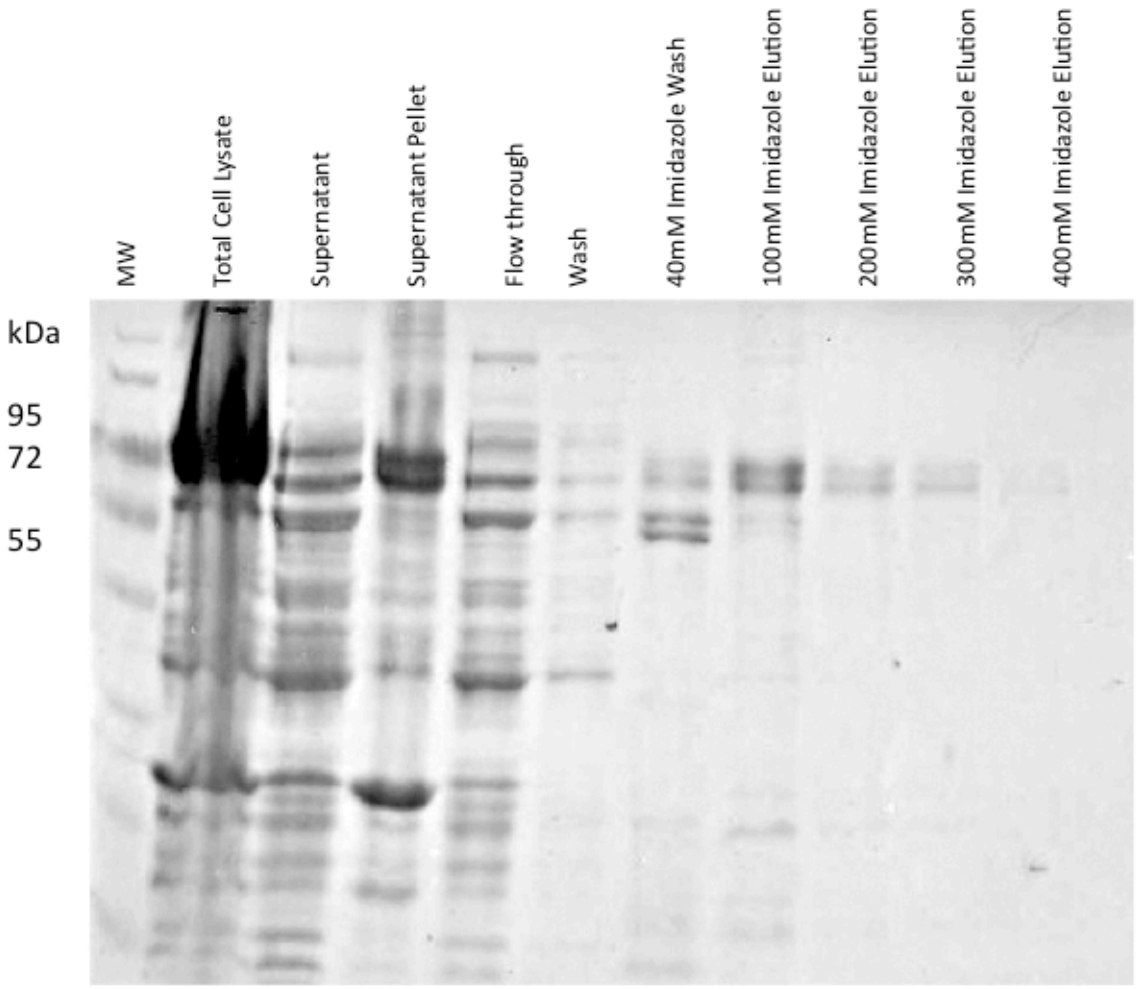


Figure 4.4. **SDS-PAGE analysis of purification of 8xHis-MDM2.** Proteins were eluted from Ni-NTA resin using a stepwise gradient elution method. MDM2 with 8xHis tagged were appeared at 95 kDa.

MCNTNMSVPTDGAVTTSQIPASEQETLVRPKPLLLKLLKSVGAQKDTYTMKEVLFYLGQYIMTKRLYDEKQ
QHIVYCSNDLLGDLFGVPSFSVKEHRKIYTMIYRNLVVVNQQESSDSGTSVSENRCHLEGGSDQKDLVQEL
QEEKPSSSHLVSRPSTSSRRRAISETEENSDELSGERQRKRHKSDSISLSFDESLALCVIREICCERSSSS
ESTGTPSNPDLDAGVSEHSGDWLDQDSVSDQFSVEFEVESLDSEDYSLSEEGQELSDEDDEVYQVTVYQAG
ESDTDSFEEDPEISLADYWKCTSCNEMNPPLPSHCNRCWALRENWLPEDKGKDKGEISEKAKLENSTQAEE
GFDVPDCKKTIVNDSRESCVEENDDKITQASQSQESEDYSQPSTSSSIIYSSQEDVKEFEREETQDKEESV
ESSLPLNAIEPCVICQGRPKNGCIVHGKTGHLMACFTCAKKLKKRNKPCPVCRQPIQMIVLTYFP

Figure 4.5-1**. Peptides of MDM2 analyzed by tandem mass spectrometry.** Peptides highlighted in green, red and yellow matched the expected peptides with a 95%, 50-95%, and >50% confidence levels, respectively.

Unused	Total	%Cov	%Cov(50)	%Cov(95)	Species	Peptides(95%)	Biological
28.54	28.54	52.95000076	42.57000089	40.52999914	Full=E3	MDM2-ubiquitin-ligase	ligase

Figure 4.5-2. **Result of electrospray ionization of of 8xHis-MDM2 using Tandem Mass Spectrometry (MS/MS).** 95% of digested peptides were identified as MDM2-ubiquitin ligase.

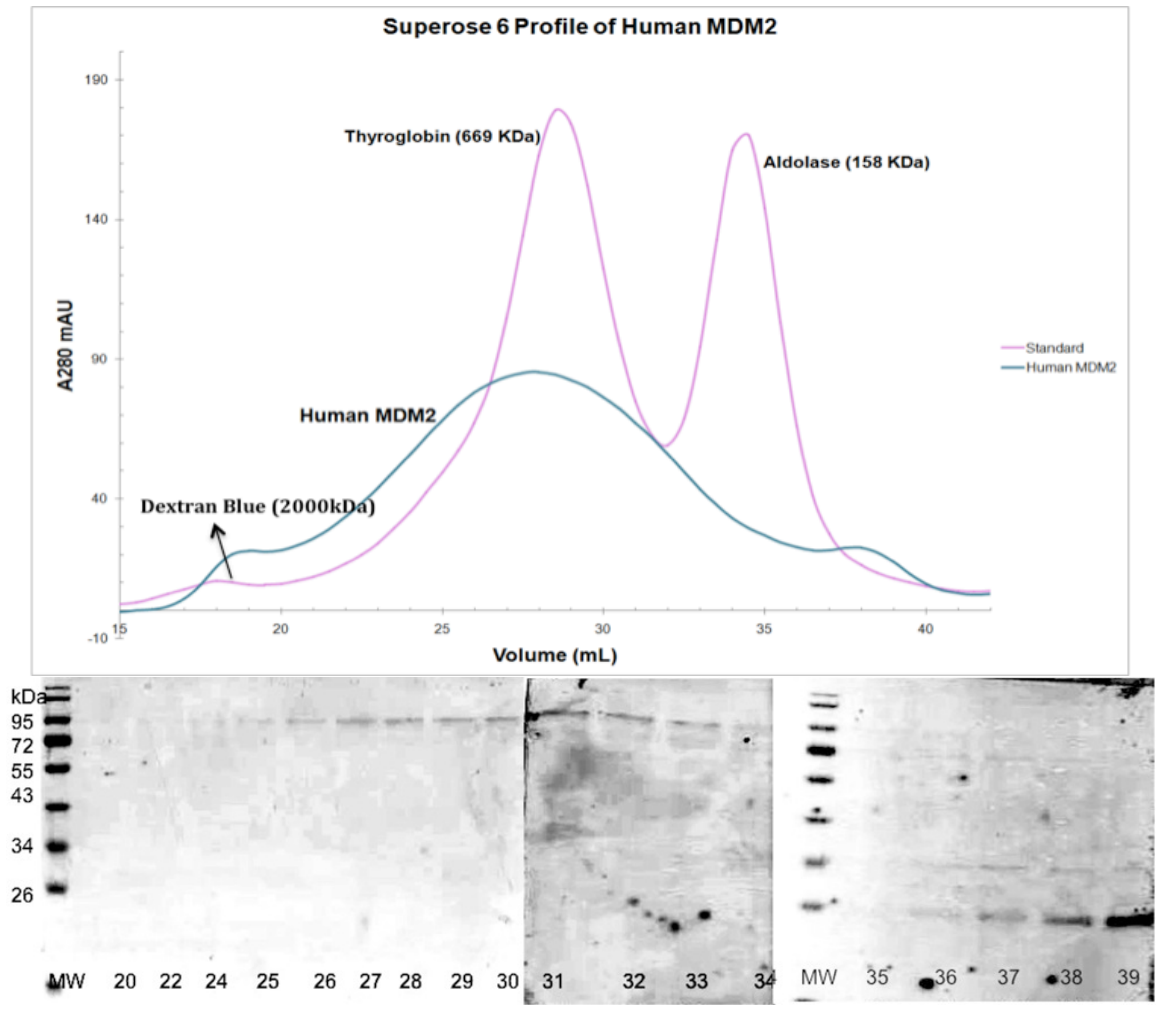


Figure 4.6. **Chromatogram of samples purifed from Superose 6 column along with SDS-PAGE ananlysis**. Samples eluted from 200 mM imidazole elution buffer was concentrated to 1 mL and loaded onto a Superose 6 column pre-equilibrated with a 500 mM NaCl, 50 mM Tris-HCl (pH 8.0), 220 mM Imidazole buffer. Purified protein eluted at fractions 24 to 32.

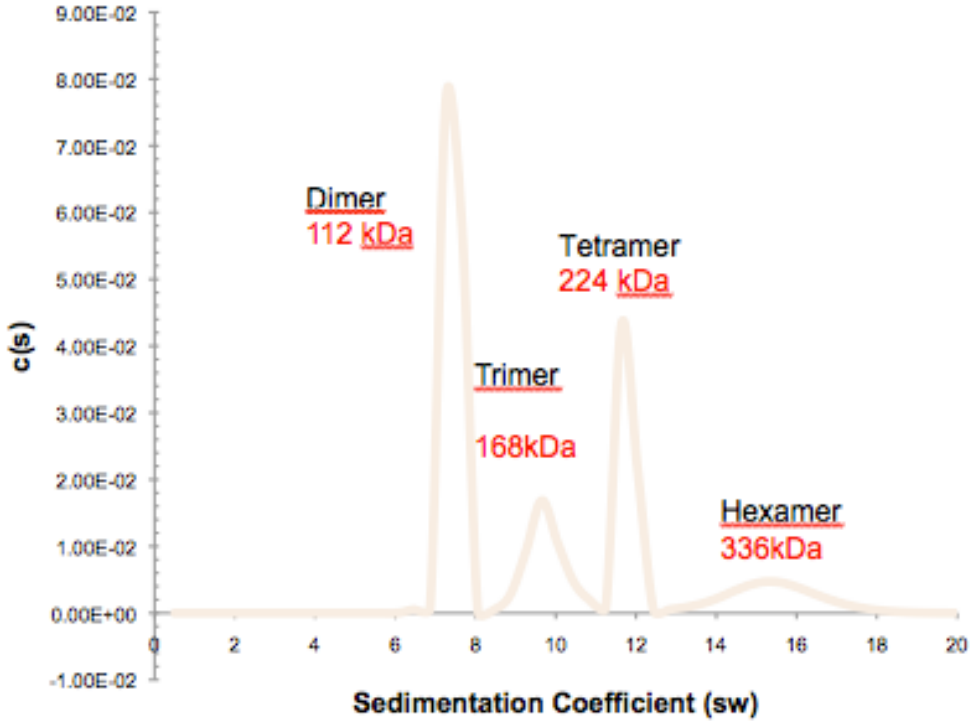


Figure 4.7. **Sedimentation Distribution of 8xHis-MDM2.** The results have shown that there are four peaks: dimer, trimer, tetramer, and oligomer.

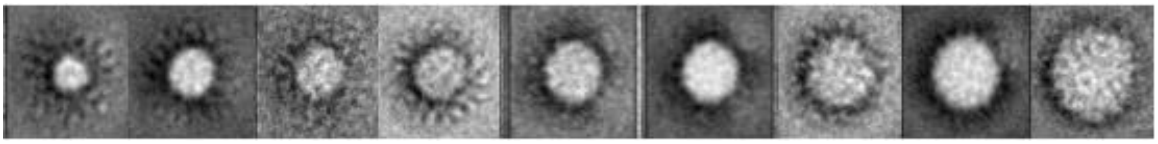


Figure 4.8. **Average of MDM2 particles.** 1727 particles were chosen by BOXER and the averages of these 10 classes were done by SPIDER using 40 pixel high filtered mask.

Discussion

Although MDM2 has been thought to be a dimeric protein for many years, we observed using gel filtration chromatography and sedimentation velocity experiments that MDM2 could form larger oligomers. Our result confirms similar studies done with the isolated MDM2 RING domain, which showed that the MDM2 RING Domain itself can assemble as supramolecular *in vitro* (Poyurovsky et al., 2007). Moreover, multiple peaks were observed in the sedimentation distribution experiment. This result is supported by the images taken with the electron microscopy, which correlate to the multiple spherical particles of different sizes. In addition, the sizes of peaks in the sedimentation distribution analysis demonstrate that the dimer of MDM2 is more abundant in the sample than the trimer, tetramer or other larger oligomers of MDM2.

Our experiments pose a question about the biological function of such supramolecular assembly. Although our *in vitro* experiments do not explain the physiological function of the large MDM2 oligomers, these experiments provide a new insight on MDM2 structure and function. One possibility is that MDM2 oligomers provide a scaffold for p53 ubiquitination during homeostasis. Also, oligomers can provide a scaffold for proteasomal degradation upon DNA damage. A similar supramolecular assembly is likely to observed in other signaling pathways that involve E3-ubiquitin ligases (Yu et al., 2006). We will continue to explore the biophysical characteristics of MDM2 and our next step for this project is to perform a single particle reconstruction of MDM2. Such approach can lead us to obtain more structural information of MDM2

References

CHENG, Q., CHEN, L., LI, Z., LANE, W. S. & CHEN, J. 2009. ATM activates p53 by regulating MDM2 oligomerization and E3 processivity. *EMBO J,* 28**,** 3857-67.

CLEGG, H. V., ITAHANA, K. & ZHANG, Y. 2008. Unlocking the Mdm2-p53 loop: ubiquitin is the key. *Cell Cycle,* 7**,** 287-92.

IWAKUMA, T. & LOZANO, G. 2003. MDM2, an introduction. *Mol Cancer Res,* 1**,** 993-1000.

JACKSON, M. W. & BERBERICH, S. J. 2000. MdmX protects p53 from Mdm2-mediated degradation. *Mol Cell Biol,* 20**,** 1001-7.

KRISHNA, S. S., MAJUMDAR, I. & GRISHIN, N. V. 2003. Structural classification of zinc fingers: survey and summary. *Nucleic Acids Res,* 31**,** 532-50.

KULIKOV, R., WINTER, M. & BLATTNER, C. 2006. Binding of p53 to the central domain of Mdm2 is regulated by phosphorylation. *J Biol Chem,* 281**,** 28575-83.

KUSSIE, P. H., GORINA, S., MARECHAL, V., ELENBAAS, B., MOREAU, J., LEVINE, A. J. & PAVLETICH, N. P. 1996. Structure of the MDM2 oncoprotein bound to the p53 tumor suppressor transactivation domain. *Science,* 274**,** 948-53.

LANE, D. P., CHEOK, C. F., BROWN, C., MADHUMALAR, A., GHADESSY, F. J. & VERMA, C. 2010. Mdm2 and p53 are highly conserved from placozoans to man. *Cell Cycle,* 9**,** 540-7.

LEHMAN, J. A., EITEL, J. A., BATUELLO, C. N. & MAYO, L. D. 2008. Therapeutic considerations for Mdm2: not just a one trick pony. *Expert Opin Drug Discov,* 3**,** 1309-1321.

MOMAND, J., ZAMBETTI, G. P., OLSON, D. C., GEORGE, D. & LEVINE, A. J. 1992. The mdm-2 oncogene product forms a complex with the p53 protein and inhibits p53-mediated transactivation. *Cell,* 69**,** 1237-45.

NICHOLSON, J. & HUPP, T. R. 2010. The molecular dynamics of MDM2. *Cell Cycle,* 9.

POYUROVSKY, M. V., PRIEST, C., KENTSIS, A., BORDEN, K. L., PAN, Z. Q., PAVLETICH, N. & PRIVES, C. 2007. The Mdm2 RING domain C-terminus is required for supramolecular assembly and ubiquitin ligase activity. *EMBO J,* 26**,** 90-101.

SHANGARY, S., QIN, D., MCEACHERN, D., LIU, M., MILLER, R. S., QIU, S., NIKOLOVSKA-COLESKA, Z., DING, K., WANG, G., CHEN, J., BERNARD, D., ZHANG, J., LU, Y., GU, Q., SHAH, R. B., PIENTA, K. J., LING, X., KANG, S., GUO, M., SUN, Y., YANG, D. & WANG, S. 2008. Temporal activation of p53 by a specific MDM2 inhibitor is selectively toxic to tumors and leads to complete tumor growth inhibition. *Proc Natl Acad Sci U S A,* 105**,** 3933-8.

SHARP, D. A., KRATOWICZ, S. A., SANK, M. J. & GEORGE, D. L. 1999. Stabilization of the MDM2 oncoprotein by interaction with the structurally related MDMX protein. *J Biol Chem,* 274**,** 38189-96.

STAD, R., RAMOS, Y. F., LITTLE, N., GRIVELL, S., ATTEMA, J., VAN DER EB, A. J. & JOCHEMSEN, A. G. 2000. Hdmx stabilizes Mdm2 and p53. *J Biol Chem,* 275**,** 28039-44.

TANIMURA, S., OHTSUKA, S., MITSUI, K., SHIROUZU, K., YOSHIMURA, A. & OHTSUBO, M. 1999. MDM2 interacts with MDMX through their RING finger domains. *FEBS Lett,* 447**,** 5-9.

VASSILEV, L. T., VU, B. T., GRAVES, B., CARVAJAL, D., PODLASKI, F., FILIPOVIC, Z., KONG, N., KAMMLOTT, U., LUKACS, C., KLEIN, C., FOTOUHI, N. & LIU, E. A. 2004. In vivo activation of the p53 pathway by small-molecule antagonists of MDM2. *Science,* 303**,** 844-8.

YU, G. W., ALLEN, M. D., ANDREEVA, A., FERSHT, A. R. & BYCROFT, M. 2006. Solution structure of the C4 zinc finger domain of HDM2. *Protein Sci,* 15**,** 384-9.